Western Kentucky University
TopSCHOLAR®

Honors College Capstone Experience/Thesis
Projects

Honors College at WKU

Spring 5-2-2011

Examining Type Ia Supernova Progenitors from Local Event Rates

Schuyler Wolff
Western Kentucky University, schuyler.wolff313@wku.edu

Follow this and additional works at: http://digitalcommons.wku.edu/stu_hon_theses

Part of the Physics Commons

EXAMINING THE PROGENITORS OF TYPE IA SUPERNOVA FROM LOCAL EVENT

RATES

A Capstone Experience/Thesis Project

Presented in Partial Fulfillment of the Requirements for

the Degree Bachelor of Sciences with

Honors College Graduate Distinction at Western Kentucky University
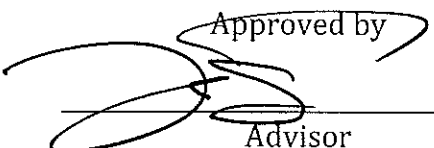
By

Schuyler G. Wolff

*****

Western Kentucky University

2011

CE/T Committee:

Dr. Louis – Gregory Strolger

Dr. Lachlan Campbell

Dr. Walter Collett

Approved by

_____
Advisor
Department of Physics and Astronomy

Abstract

We present the recalculation of the rates of supernovae in local, low redshift ($z \leq 0.1$) from the Nearby Galaxies Supernovae Search Project (Strolger, 2003) using an improved baseline designed to maximize SNe yield. Approximately 15 additional SNe of various types and ages have been discovered from the dataset and added to the 42 SNe already detected. This sample is sufficient to obtain an accurate rate of SNe in the local universe. The rates are weighted by volume, total light, and host galaxy type. Further spectroscopic data for the progenitor galaxies of each event will allow us to compare the rates using various galaxy properties. Contributions included an estimate of the precision and depth of the survey with false supernovae, and estimated luminosity function using literature estimates, and determining the control times for the survey to correct for the cadence and sensitivity of the survey. We present a detailed description of the resurveying of the NGSS dataset, the rate calculations, and the preliminary results. We obtain a B-band rate of $0.220 \, century^{-1} [10^{10} L_{\odot}(B)]^{-1}$. This roughly corresponds to 1 SNe Ia every 400 - 500 years in a galaxy like the Milky Way.

Keywords: Physics, Astronomy, Astrophysics, Extragalactic, Type Ia Supernova, Local Galaxies

para mis padres y mis hermanitas

Acknowledgements

Vita

Education

- High School Diploma (2008), Carol Martin Gatton Academy of Mathematics and Science of Kentucky. Bowling Green, KY. Note: Graduated with Honors in the Inaugural class.

- High School Diploma (2008), Oldham County High School, Buckner, KY. Note: Graduated with honors.

- Bachelor of Science, Physics & Astronomy, Concentration in Astrophysics. Date of graduation: May 2011, Western Kentucky University, Bowling Green, KY.

Work Experience

- Undergraduate Research Assistant, Western Kentucky University, Bowling Green, KY (2008-present): *Worked on both group and individual research projects concerning applications of supernovae in cosmology and involving data searches, cataloguing, and programming* (See **Undergraduate Projects**).

- Physics and Mathematics Tutor, Carol M. Gatton Academy of Mathematics and Science, Bowling Green, KY (2009-present)

- Deutscher Akademischer Austausch Dienst Research Internships in Science and Engineering program summer intern (2009): *Worked in Microlensing studies at*

the Max Planck Institute for Astrophysics and the Institute for Astrophysics at Göettingen University in Germany (See **Undergraduate Projects**).

- National Science Foundation, Research Experiences for Undergraduates program, Harvard-Smithsonian Astrophysical Observatory summer internship (2010): *Worked on a project in solar-system orbital dynamics.* (See **Undergraduate Projects**)

Awards and Activities

- Western Kentucky University President's Scholarship (2007-present)

- Gatton Academy Undergraduate Scholarship (2007 - present)

- WKU Honor's College Student (2007 - present)

- WKU Ogden College of Science and Engineering Dean's List (2007- present)

- NASA Kentucky Space Grant Consortium Undergraduate Scholarship (2009-2010)

- Distinction and runner-up for the Marsh White Undergraduate Presentation Award, the 77th meeting of the Southeastern Section of the American Physical Society (2010)

- President of the WKU Society for Physics Students (2010 - present)

- Executive Officer of the Hilltopper Astronomy Club (2010 - present)

- Member of Sigma Pi Sigma and Pi Mu Epsilon (inducted 2010)

- Junior member of the AAS (2010 - present)

- Randall Harper Award for Outstanding Research in Physics and Astronomy (2010)

- Doug Humphrey Award for Outstanding Service in Physics and Astronomy (2011)

Undergraduate Projects

- **Nearby Galaxy Supernovae Search (NGSS):** This survey began in 1998 and was designed to detect low redshift supernovae of all types. Four successful search campaigns were conducted using the KPNO 0.9-meter telescope and the Mosaic North 8k X 8k camera array. Using improved baselines between template and search images, we have added approximately 20 supernova to the original sample of 42 supernova of various types.

- **Large Survey Follow Up:** This project was designed test the ability of a 1-m class telescope to obtain supernova classification through photometric light curves. This was done by collecting photometric light curves of type Ia supernova candidates using the WKU-lead 1.3-meter Robotically Controlled Telescope, in Tucson, AZ. The sample was taken from the unclassified objects in the Catalina Sky Survey and Palomar Transient Factory datasets.

- **Supernova HST-MCT under Cosmic Assembly Near-infrared Deep Extragalactic Legacy Survey (CANDELS):** My current work-study is as a data reviewer for the CANDELS supernova survey (PIs: Adam G. Riess and Sandra M. Faber). I participate in the real-time pixel-by-pixel review of accumulating CANDELS data to find very high-redshift supernovae (particularly type Ia supernovae) in the $1 < z < 2.5$ regime. Thus far, I am also assisting in the development and training of a automated "sniffer" to robustly discover these events without significant human intervention.

- **Supernova Rate Calculator:** Here I designed a supernovae rate calculator to be used in collaboration with the sample from the Nearby Galaxies Supernova Search project. Contributions include a control time calculation, a luminosity density function, and an event rate weighted by host galaxy properties including metallicity, star formation rate, and stellar population ages.

- **Gravitational Microlensing:** I served as a DAAD Rise intern at the University of Göttingen in Göttingen, Germany. There I worked with Marcus Hun-

dertmark using the MONET North and South telescopes to track microlensing events listed in the OGLE and MOA candidate lists. Additional contributions included a set of IDL programs to fit microlensing light curves with a Point Source Point Lens model in order to determine the mass of orbiting extrasolar planets.

- **Solar System Dynamics:** During a summer REU opportunity with the Smithsonian Astrophysical Observatory I worked with Dr. Ruth Murray-Clay on simulations of the Kuiper Belt. The project was designed to determine if a qualitative understanding of the impacts of Neptune on the developing Kuiper Belt could produce the dynamical populations seen today. Different behaviors of Neptune were examined including an outward migration and damping of the orbit in both eccentricity and inclination.

Publications and Presentations

- Scott, J., Kintzel, E., Strolger, L., & Wolff, S. 2010, APS Meeting Abstracts, 27

- Wolff, S., Strolger, L., Pease, A., & Gott, A. 2010, Bulletin of the American Astronomical Society, 42, 358

- Pease, A. M., Strolger, L., Wolff, S., & Gott, A. 2010, Bulletin of the American Astronomical Society, 42, 356

- Strolger, L.-G., van Dyk, S., Wolff, S., Campbell, L., Sadler, S. M., & Pease, A. 2011, NOAO Proposal ID #2011A-0416, 416

- Wolff, S., Murray-Clay, R., & Dawson, R. 2011, "Investigating the Dynamical History of the Solar System", 217th Meeting of the American Astronomical Society

- Wolff, S., & Strolger, L. 2010, "Investigating Type Ia Supernovae Progenitors from Local Rates", 77th Annual Meeting of the Southeastern Section of the

American Physical Society, Baton Rouge, LA.

- Wolff, S. G. 2008, "Nearby Galaxy Supernova Search I: Fuzzy Exploding Stars on a Computer Screen", 38th Annual WKU Student Research Conference, Bowling Green, KY.

- Wolff, S. 2009, "The Origins of Type Ia Supernovae From Rates in the Local Universe", Conference for Undergraduate Women in Physics, Lincoln, NE.

- Pease, A. M., Strolger, L., & Wolff, S. G. 2008, "Discovering and Cataloging Variable Objects in the Nearby Galaxies Supernova Search data", 19th Argonne Undergraduate Symposium, Argonne, IL.

- Pease, A. M., Strolger, L., & Wolff, S. G. 2008, "Reanalyzing the Nearby Galaxies Supernova Search Data" , Kentucky Academy of Sciences meeting, Lexington, KY.

- Pease, A. M., Strolger, L., & Wolff, S. G. 2008, "Reanalyzing the Nearby Galaxies Supernova Search Data", 14th Annual Kentucky EPSCoR Conference, Cyberinfrastructure - Connecting with the Future, Louisville, KY.

Table of Contents

List of Figures

List of Tables

Chapter 1

Introduction

When Einstein went about creating his General Theory of Relativity in 1917, he found it was necessary to include a 'fudge factor' he named the Cosmological Constant in order to produce a static universe. Einstein later went on to call this inclusion his 'Greatest Blunder' when it was discovered that the universe was far from static. Just as the theories of relativity changed the way we think about space and time, the discovery of the current epoch of expansion changed views of cosmology.

Evidence for the acceleration of the expansion of the universe was first published in 1998 by the High-z Supernovae Search Team using distance measurements derived from observations of Type Ia supernovae (Riess et. al. 1998). A plot of distance as a function or redshift (recessional velocity) revealed a trajectory inconsistent with a matter-filled universe as seen in the SNIa Hubble Diagram (Figure 1.1). The implied acceleration could not be explained as the result of momentum caused by the Big Bang. Some other force must be responsible. The term Dark Energy has been coined to explain this uncharacterized force responsible for the accelerated expansion. Attempts to quantify dark energy continue.

Since the initial discovery of dark energy through the use of Type Ia supernovae (SNe Ia), other tools have been used to further support its existence. Two convincing proofs for dark energy jointly come from the Cosmic Microwave Background (CMB; Spergel et al. 2007) and signatures from Baryon Acoustic Oscillations (BAO; Eisenstein et al. 2005) that show an evolution of structure inconsistent with a universe
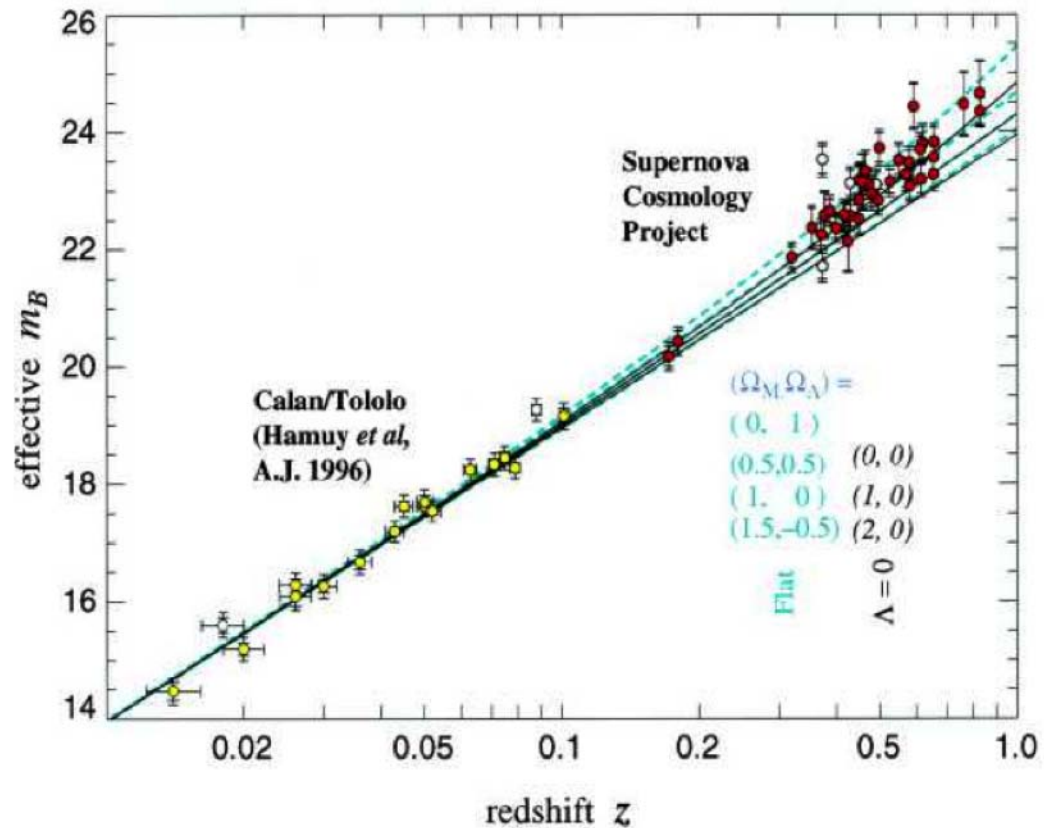
Figure 1.1: From Perlmutter et al. 1999, evidence for dark energy as deduced from observations of Type Ia SNe. In 1998 distance measurements were made using Type Ia supernovae that led astronomers to believe the Universe was expanding, and the expansion was accelerating. A plot of effective absolute magnitude in the B-band as a function of redshift demonstrates that observational evidence from SNe Ia strongly favors an open universe.

dominated strictly by gravitational effects. The concordance is that dark energy makes up $\sim 70\%$ of the density of the universe, however, we lack a solid theoretical framework to describe what it is, and therefore must continue to rely on observations to better understand its nature. The current measures from SNe Ia, CMB, and BAO are all supportive of an equation of state, $w = -1$ and $w = 0$ (to within 7%), which implies that dark energy is an invariant cosmological constant (Riess et al. 2007). But demonstrating $w \neq -1$ or $w' \neq 0$ would be a tremendous breakthrough in our understanding. SNe Ia remain our best tool for this test, from their direct sensitivity to dark energy, and their extraordinary precision in distance through empirical corrections. However, it is these empirical corrections and the physics that lead to them which is now the focus in further narrowing the dark energy error budget.

1.1   Supernovae and their use as Standard Candles

Supernovae can be separated into several categories according to differences between the characteristic photometric light curves and optical spectra. Type I are distinguished from type II by the absence or presence, respectively, of Hydrogen lines in the spectra. Type II supernovae are classified by the shapes of their light curves. Type II-L have light curves with nearly linear decay where type II-P show a noticeable plateau in the light curve. All of the type II category objects are core collapse events. These events are the result of a massive star that has used up the elemental fuel within the core leaving only nickel and iron. At that point, the gravitational pressure is no longer supported by the radiation pressure from fusion in the core and a collapse occurs. A shock wave results and the envelope is kinetically exploded outward, additionally propelled by neutrinos. Within the category of Type I supernovae, there are three subcategories labeled Ia, Ib and Ic. Type Ib and Ic SNe are also thought to be core collapse events. The absence of Hydrogen in the spectra is a consequence of the age of the progenitor stars. Parents of Type Ib/c SNe are older red giant stars with outer Hydrogen envelopes that have eroded away.

In contrast, the detailed mechanism to produce SNe Ia is not well understood. It is generally believed that SNe Ia result from a thermonuclear explosion of white
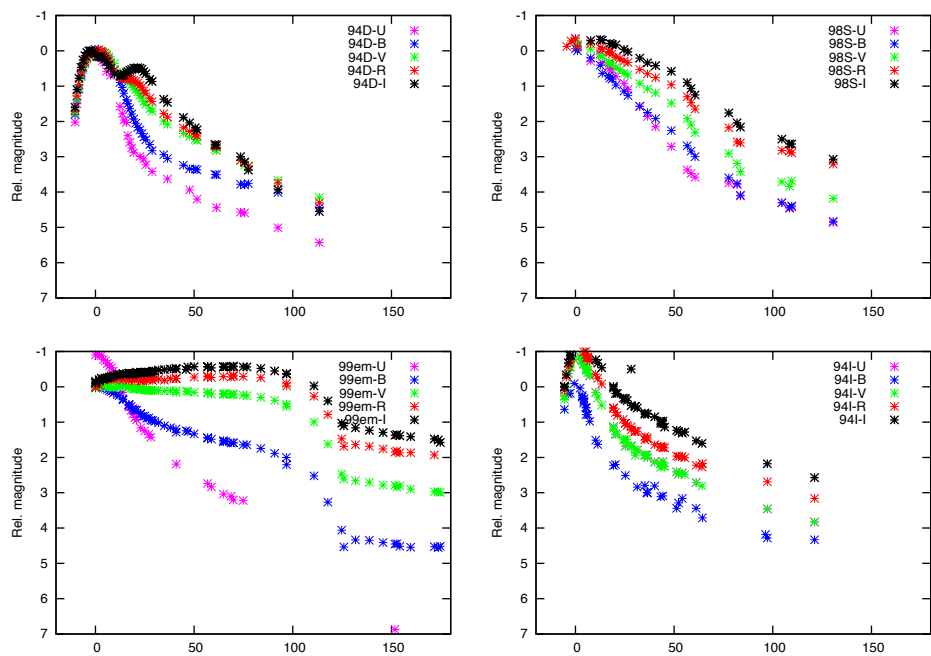
Figure 1.2: Empirical light curves shapes scaled by a relative magnitude. SN1994I for type Ib/c supernovae, SN1994em for type II-P supernovae, SN1998S for type II-l supernovae, and SN1994D for type Ia supernovae.
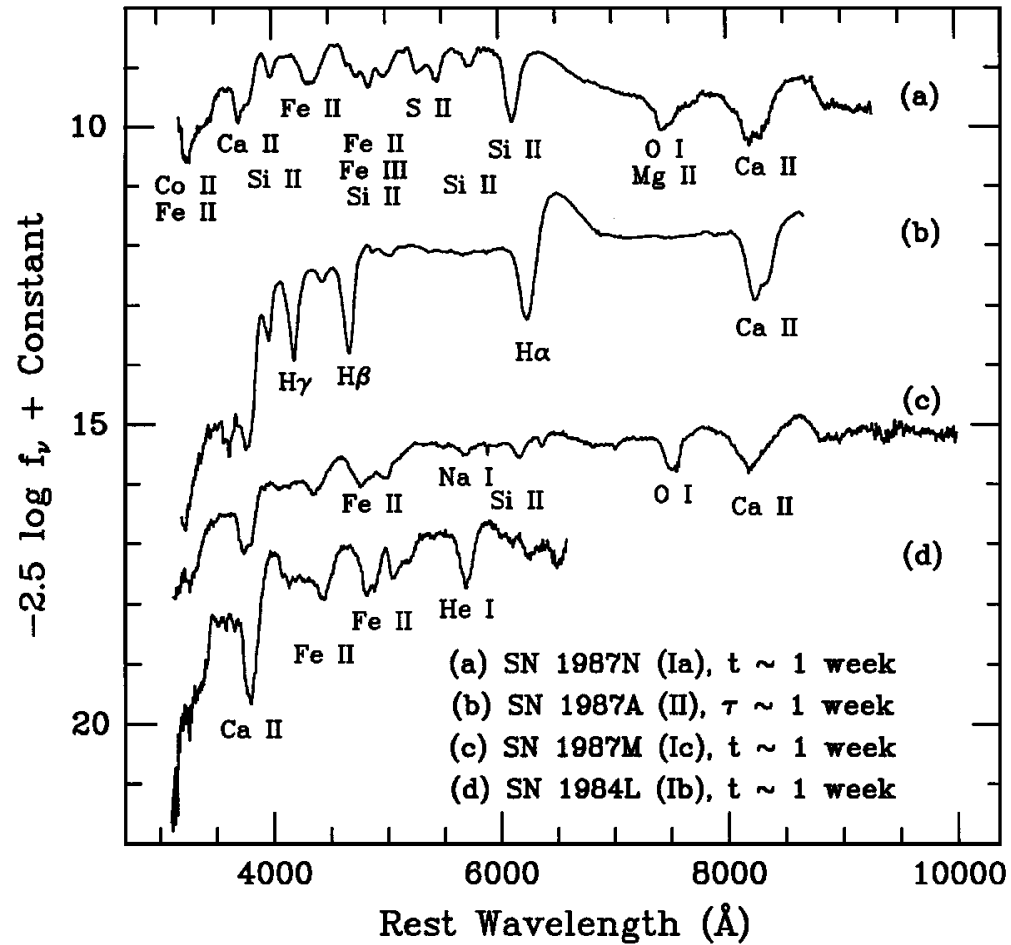
Figure 1.3: From Filipenko 1997, spectra of SNe showing early-time distinctions between the four major types and subtypes. In this review, the variables t and τ represent time after observed B-band maximum and time after core collapse, respectively. The ordinate units are essentially AB magnitudes as defined by Oke & Gunn (1983).

dwarf stars. The leading model uses a white dwarf star that is accreting matter from a nearby red giant. Eventually, the white dwarf will reach the Chandrasekhar mass limit of $M \cong 1.4 M_\odot$, a theoretical limit based on the Pauli exclusion principle beyond which the gravitational pressure will overcome the electron degeneracy pressure within the core. As the star collapses, conditions within the core becomes hot and dense enough to thermonuclearly ignite carbon through fusion. This process quickly uses up all the material in the star. The resultant explosion produces an extremely bright object lasting on the order of a few months in the measured rest-frame.

The collective group of core collapse events tend to be fainter than Type Ia thermonuclear events by several factors of ten, and have a wider spread in measurements of the peak magnitude. Type Ia events can be detected at much larger distances than core collapse events, making them useful tools in the study of the evolution of the early, distant universe. Because SNe Ia all result from the carbon fusion of the same amount of material ($1.4\ M_\odot$), the peak absolute magnitude of these events is $M_B \cong -19.3 \pm 0.03$ corresponding to total energy outputs of $1 - 2 \times 10^{44}$ Joules with little scatter. Consequently, the peak magnitudes seen in the supernovae light curves can be used to calculate the distance via an application of the inverse square law as shown in equation 1.1.

$$d_L = \left(\frac{L}{4\pi F} \right)^{\frac{1}{2}} \tag{1.1}$$

Here, L is the intrinsic luminosity, and F is the absorption-free peak flux observed for the SN. This allows the use of SN Ia as cosmological distance indicators or standard candles.

Distances found using the supernovae method have very high accuracy with a discrepancy of only 22 percent for very large distances. Correlations have been drawn between the peak luminosity of these events and the shapes of their light-curves (Phillips 1993), which have been vital to exploring the expansion history of the Universe (via the Hubble diagram). Though there is a spread in the peak magnitude of SNe Ia of ± 0.2 mag, there is a strong correlation between the maximum bright-

ness of the SNe Ia event and the rate of decline of the luminosity as illustrated in the light curves. Multicolor light curve shape (MLCS) methods and stretch (Δm_{15}) methods can be used to derive a peak magnitude from the light curve shapes of observed SNe Ia. Using these correlation methods, uncertainties of 7 % can be obtained. The scatter in peak magnitude could be explained as evidence in a discrepancy between the progenitor masses or differing explosion mechanisms. Event rates can aid in the understanding of this disparity with the aim of further constraining the error in cosmology measurements derived from observations of SNe Ia.

1.2 Rates in the Local Universe

The nearby rate of supernovae is an important determination for many areas of astrophysics. Supernovae represent an important stage in the life cycles of stars, and the evolution of galaxies. Constraining the rate of supernovae would place a limit on both the amount of chemical enrichment in the interstellar medium and on stellar evolution models (Van den Bergh et al. 1991) though enrichment of stellar nurseries. The investigation of SNe rates of all types is important to gain an understanding of the status of chemical enrichment via star-gas-star processes.

The detection frequency of SNe Ia events is typically higher than core collapse (CC SNe) events because the Ia events are much more luminous. However, it is thought that the CC SNe are inherently more frequent. Here, we focus on SNe Ia rates because of their importance to cosmology studies.

As previously stated, the mechanisms that produce SNe Ia are not well understood. The correlations made between the peak magnitudes and the decline rate of the light curves may be incorrect. This would drastically effect precision cosmology measurements made using SNe Ia. By investigating the event rate of these objects, we can gain a better understanding of the conditions necessary to produce these events and any dependence on progenitor properties such as age and metallicity.

There have been many attempts to constrain the rate of supernovae of all types in the local universe. The first attempt by (Zwicky 1938) gave the mean frequency of SNe in an average galaxy like the Milky Way to be 460 years. These early attempts

were limited by unaccounted for observational biases. Specifically, Zwicky failed to correctly calculate the control time, or effective time of SN detectability, for his survey. Additionally, the inability of photographic plates to resolve SNe from the bright central regions in galaxies would have further reduced his results by ~ 20 %. With the development of CCD devices and larger sample sizes, uncertainties have been reduced and current rate estimates provide sufficient means to constrain the progenitor systems of SNe Ia events.

Supernovae rates in the nearby universe are widely varying. As an anecdotal comparison, we examine two galaxies; the Milky Way ($L \approx 2.6 \times 10^{10} L_\odot$) and Arp 299 ($L \approx 4.5 \times 10^{10} L_\odot$). The most recent observed supernova in the Milky Way galaxy was Kepler's Supernova, first observed in 1604. [1] In the last millennium, there were only six historically recorded supernovae of all types in the Milky Way. This results in an average general supernovae rate of just under one per 200 years. Conversely, the galaxy merger system Arp 299 (IC 694 + NGC 3690) has produced 9 supernovae in just the past decade. Radio emission tracking SN remnants in Arp 299 suggests a supernova rate ranging from a few tenths to a few supernovae per year (Neff et al. 2004). This variance points to other factors in normalizing SN rates, not just the number of stars (or $10^{10} L_\odot$). This is further evidenced by the metallicity of the Milky Way suggests a rich history of chemical enrichment from supernovae that is not seen in current rate measurements.

Studies of SN Ia rates at low-z have shown that late-type galaxies are more prolific producers of SNe Ia than early-type galaxies of the same mass (Hamuy et al. 2000, Mannucci et al. 2005). It remains unclear why this is so. One possible explanation for this discrepancy could be a dependency of SN Ia rates on metallicity variations in the host environments. There is some expectation that the progenitor metallicity at formation should affect the luminosity of the product SN Ia (Timmes et al. 2003), possibly with adverse effects on luminosity corrections, including MLCS stretch or similar methods, that may also evolve with cosmic time (e.g., metallicity dependent Hubble residuals). It is believed that the metallicity of the progenitor system would

---

[1] The Cassiopeia A remnant is a very bright radio source but the event, which occurred ~ 1700, went unseen.

have an inverse relationship with the luminosity of the SN Ia event. As the metallicity increases, the increased amount of Nitrogen present would limit the ^{56}Ni decay. The interpretation thus far is that $\geq \frac{1}{2}$ of SNe Ia are "prompt" events, exploding within ≈ 500 Myr of progenitor formation. But prompt SNe Ia pose a potential problem for precision SN Ia cosmology.

The metallicity of the host environment could also directly effect production efficiency. Recall the assumed white dwarf progenitor with a neighboring red giant. A higher metallicity white dwarf star would display line blanketing in which the heavier atoms cause absorption lines in the UV spectrum resulting in a lower over all flux. Thus, a higher metallicity would produce SNe Ia events with a lower luminosities. Conversely, increasing the accretion rate due to a higher metallicity would ignite fusion on the surface of the white dwarf. This would limit matter accretion to the core and prohibit the system from reaching the mass limit ($1.4M_\odot$) resulting in recurrent nova. Inherent CNO-cycle product enrichment may be necessary to "pump-up" the white dwarf's stellar wind to allow for steady mass accretion, which prevents alternative end-products such as H or He flashes, or accretion induced core-collapse supernovae (Kobayashi et al. 1998). Thus, an increased metallicity could decrease the peak magnitude of a supernovae, but it could also increase the rate (Kessler et al. 2009, Riess et al. 2007). The most distant SNe Ia to date (to $z \approx 1.8$; Strolger et al. 2010) suggests instead that SNe Ia are very delayed events, requiring ~ 3 Gyr to develop from a burst of star formation. These results are more favorable for cosmology, which is unsupportive of strong metallicity Hubble residuals as progenitor metallicities are "locked-in" at much earlier cosmic epochs. Thus far, large delay models have been difficult to reconcile with the low-z rate trends with galaxy types. Confirmation that rates are highest in metal-rich galaxies when weighted by stellar ages or star formation rates would provide proof that SN Ia are sensitive to the local metallicity variations in that a minimum metallicity must be met to efficiently produce SNe Ia.

Chapter 2

The Nearby Galaxies Supernovae Search Project

2.1 Observational Strategy

The supernova sample for this project came from the Nearby Galaxy Supernova Search. The purpose for this survey was to detect and study low redshift supernovae of all types. Data for this survey was taken from 1999 to 2001 with the 0.9-meter telescope at Kitt Peak National Observatory (KPNO) near Tuscon, AZ. The photometric campaign consisted of four epochs each spaced a month apart with the Mosaic North 8k X 8k camera array (Mosaic I). Each of the 5 - 8 night campaigns have allowed the search of 250 fields (each nearly 1 degree sq.) for a total sky coverage of approximately 493.56 square degrees along the celestial equator and out of the Galactic plane to limiting magnitudes of ~ 21 in the R-band. For comparison, the constellation Orion occupies ≈ 50 square degrees of sky. At the time of it's completion, the NGSS project was the largest campaign for low-z supernovae.

The photometric data was reduced via standard IRAF techniques in the MSCRED package. Each image was zero corrected to remove detector bias induced in reading the array. The images where then flat subtracted to account for the illumination on the chip. Multiple exposures of the same field were taken in order to maximize signal-to-noise and remove pixel defects and cosmic rays. Stellar catalogues were
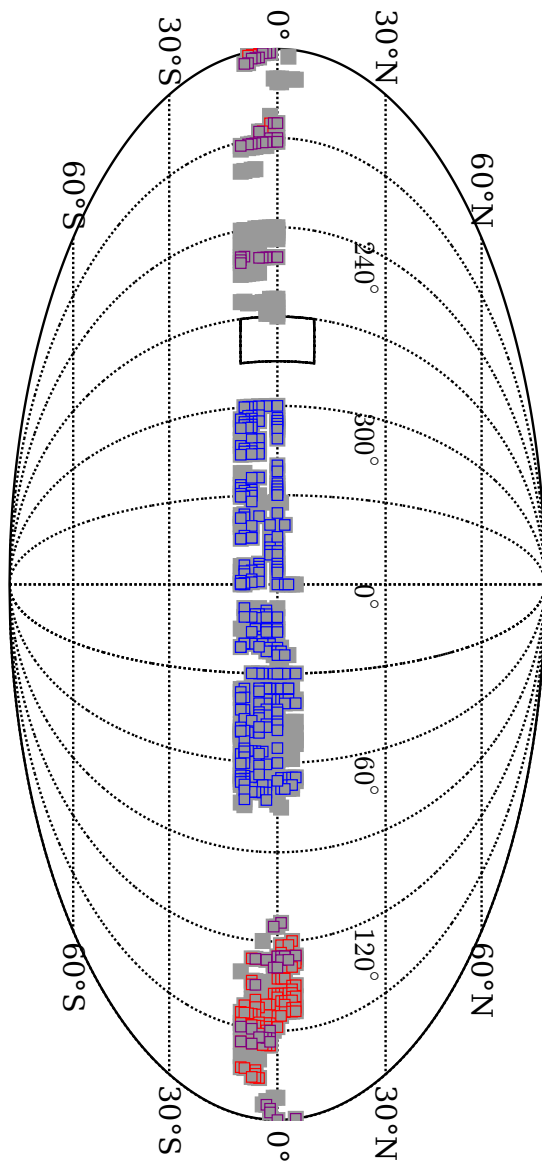
Figure 2.1: The field coverage for the Nearby Galaxies Supernovae Search. Grey is the template, blue is second epoch, red is third epoch and purple is fourth epoch.

developed in order to match images of the same location. The registered images were then combined in order to reduce the effects of hot pixels and cosmic rays. Combined template and search images for each field were constructed using these methods. Because seeing conditions changed between the different epochs, a correction to the point spread function was made to correct for changes in the atmospheric turbulence. After this process, the combined template image was subtracted from the combined search images. The subtracted image then contained only transient objects and core residuals.

2.2 Searching for Supernova

When the survey was originally conducted, the SNe search had to be completed in real time to obtain candidates for follow up observations. The subtractions for all tiles were searched by eye using DS9 software. The time between the exposures for the template and search images (baselines) varied widely. The cadence of the survey had a large effect on SNe yield. In the original survey, 42 supernovae of various types with 18 type Ia supernovae were discovered with $\bar{z} \approx 0.11$ for the sample.

A resurveying of the data was recently conducted using improved searching cadences in order to maximize the SNe yield. During the resurveying, we focused on detecting any additional SNe and on producing a catalogue of all transient objects. The majority of the baselines used previously had been ≤ 30 days. This is within the time frame expected for a SNe event. By lengthening our baselines, we were able to increase the contrast between the search and template images which served to increase our detection efficiency. During the resurveying, we focused on improving our supernovae yield and on producing a catalogue of transient objects. The longer baselines allowed us to discover an additional 20 SN resulting in a total sample size of approximately 60 objects.

During this second search, methods were employed to better understand our detection efficiency. Each image was given a quality ranking from 1 to 3 based on the condition of the chip and the seeing conditions on the night. The results from the rankings were included in the control time (effective survey time) calculations. In
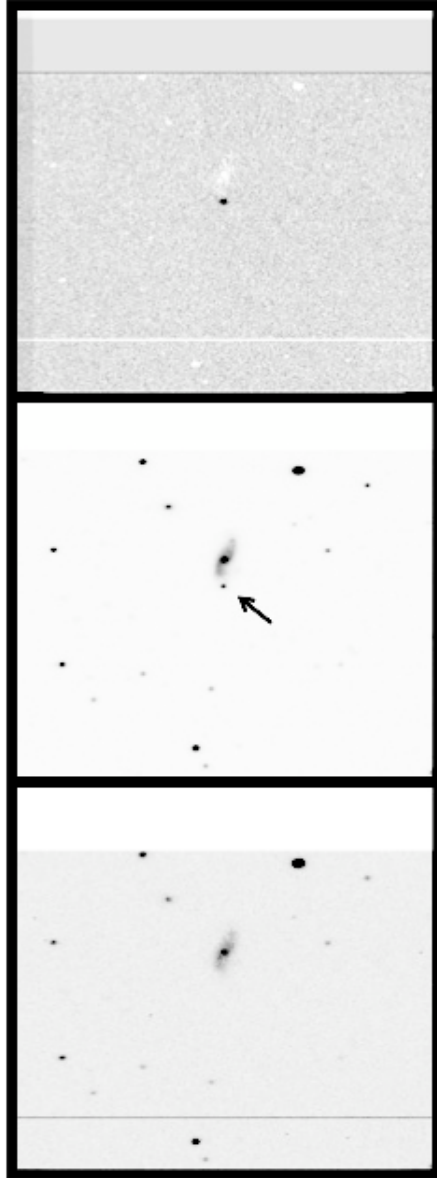
Figure 2.2: The template, search, and subtraction images (from the top down) for SN candidate Laurel shown with host galaxy NGS081501.
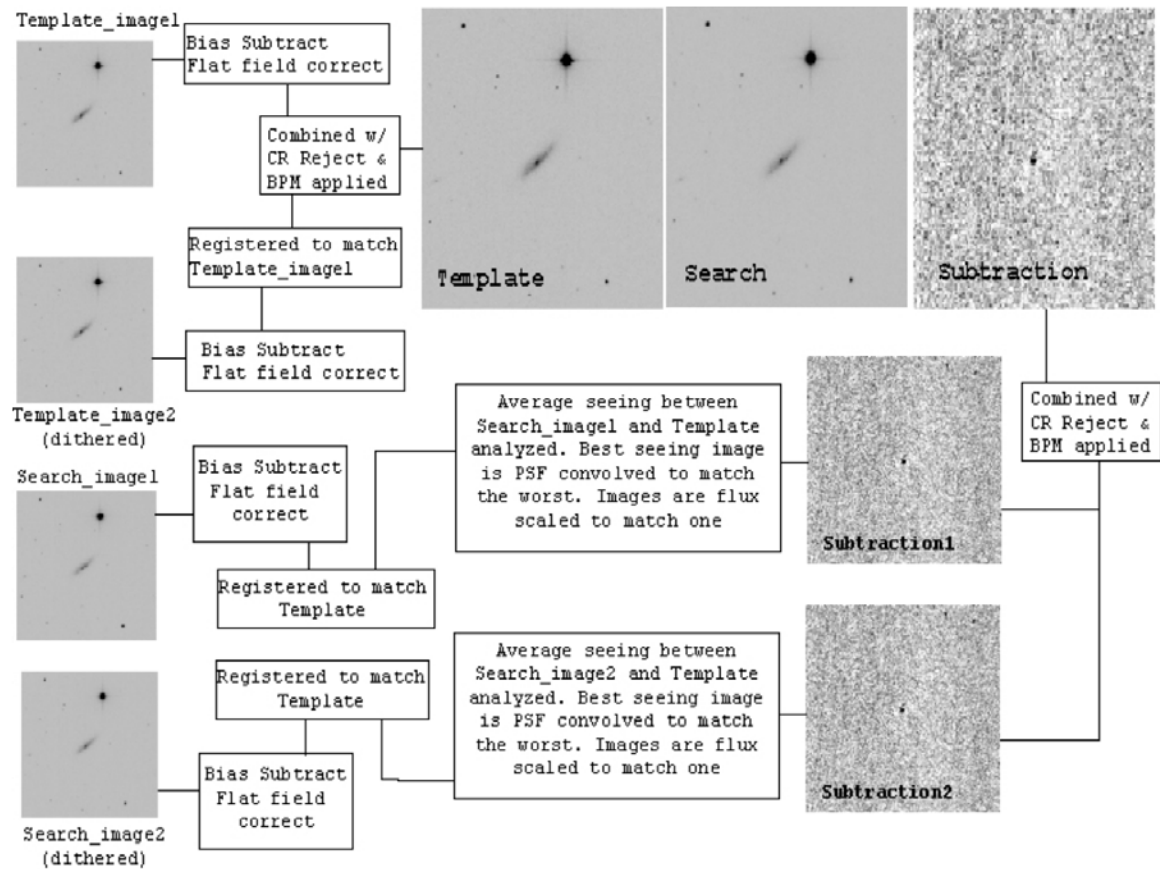
Figure 2.3: Schematic of the method used to create the subtracted images of each field. The original images were bias subtracted and flat field corrected. Images of the same field were combined. A subtracted image was created from the template and search images.

28
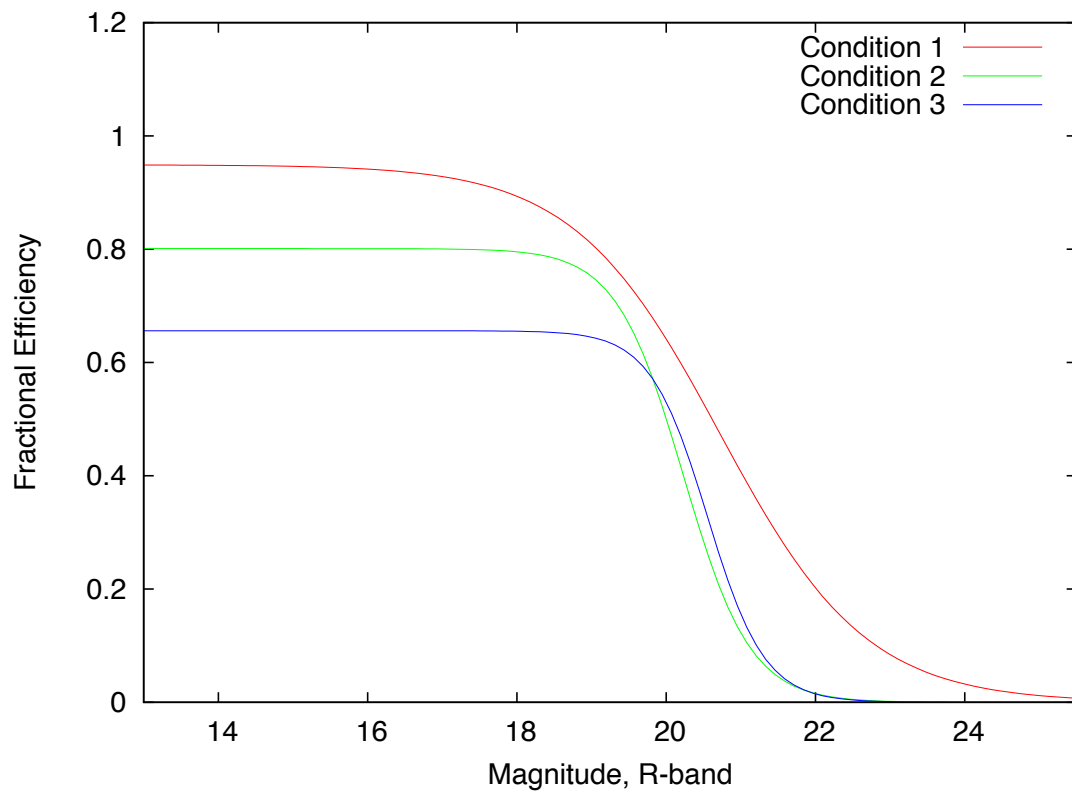
Figure 2.4: The searching efficiency curves as a function of the R-band magnitude for the different quality rankings.
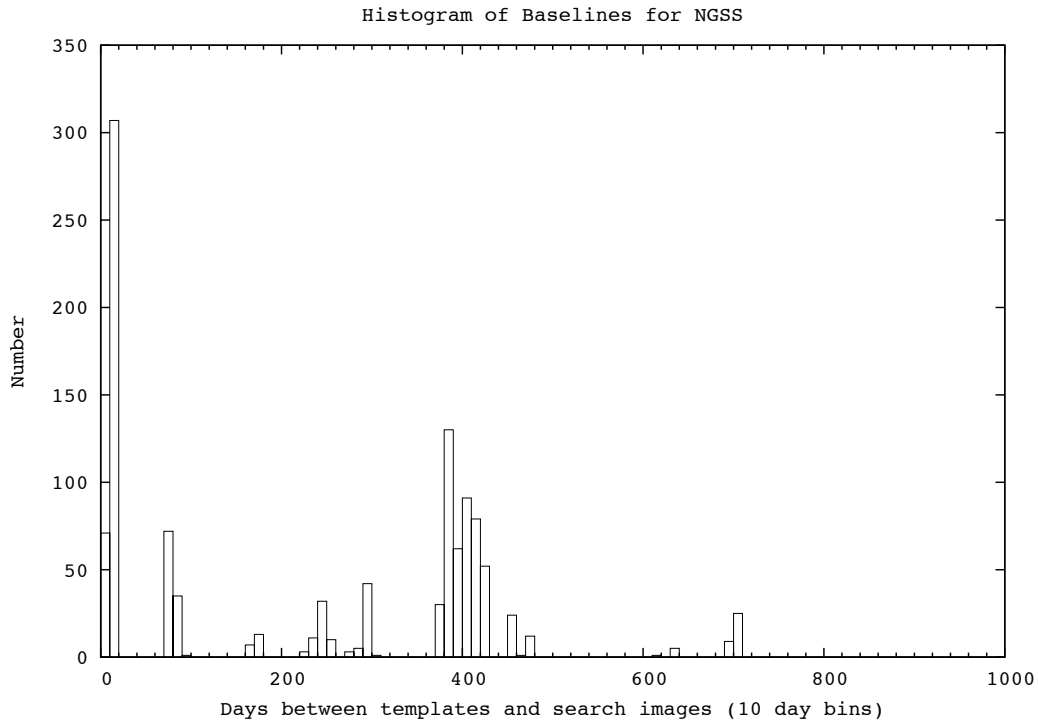
Figure 2.5: Histrogram of the Baselines used in the Nearby Galaxies Supernovae Search. Many of the baselines were ≤ 30 days.

addition, we included a double blind test to determine the detection efficiency of the searching team. A collection of fake supernovae of various magnitudes were imbedded throughout the image data. Each searcher was able to compile a probability of their ability to detect a supernovae of a given apparent magnitude. It was determined that the detection efficiency was nearly 100 % above the limiting magnitude of $R \sim 20$ falling to 0 % below the limiting magnitude shown in Figure 2.4. The probability of detection was also included in the control time calculations.

2.3 SN Follow Up

Searching through the subtracted images provided a catalogue of SNe candidates. In order to determine the type of each candidate, additional data was needed. A supernovae type identification can be obtained through photometry or spectra of the candidate. Spectral classification is more robust but requires more time. 2 - 3 nights of spectra were obtained following each search epoch at the Kitt Peak National Observatory (KPNO) Mayall 4-m and the Cerro Tololo Inter-American Observatory (CTIO) Blanco 4-m telescopes. The optical spectra obtained provided information about the type and evolutionary age of each candidate and rejected those candidates which were not supernovae.

Attempts were also made to obtain photometric light curves. For several months after each search epoch, photometric data was obtained from the 0.9-meter, 1.5-meter, and YALO 1.0-meter telescopes at CTIO. Sampling for each supernovae was constrained to 3-5 days. This data provided well-sampled light curves. A photometric classification could be obtained by examining the shape of the lightcurve. When objects were sufficiently bright, infrared photometic data were also obtained using the Swope 1.0-meter and duPont 2.5-meter telescopes at Las Campanas Observatory, and the YALO 1.0-meter telescope at CTIO.

For the new additional candidates obtained during the resurveying of the data, photometric and spectroscopic data are unattainable as the SNe event has long since faded. However, spectra of the host galaxies for these events can provide us with a well constrained spectroscopic redshift. Using these distances and the apparent magnitude, we are able to determine the absolute magnitude and put some constraint on the SNe type.

31

Table 2.1: SNe candidates from the NGSS survey. Spectroscopic and photometric redshifts are given. Type determinations have been made when possible.

SN	A.K.A	Type	Disc. Date	RA(2000)	DEC(2000)	z approx.	R mag approx.
—	Fozzie	??	11/13/00	00:33:26.83	-09:17:14.4	??	20.7
2000em	Animal	II-pec	11/16/00	00:35:29.82	-02:39:27.4	0.0194	18.3
2000en	Rizzo	Ia	11/16/00	00:43:08.37	-00:23:17.6	0.150	20.2
2000ff	Swedish Chef	Ia?	11/14/00	00:45:24.72	-03:16:47.2	0.0721	19.5
1999en	Corinne	Ia	10/03/99	01:15:29.70	-04:30:48.2	0.16	20.5
1999eq	Minnie	II	10/03/99	01:19:22.70	-03:36:19.8	0.045	20.3
2000fg	Janice	??	11/16/00	01:24:31.36	-10:23:46.2	??	18.8
—	George	??	11/16/00	01:26:21.66	-01:16:27.4	0.037	18.6
1999eo	Khadijih	Ia	10/02/99	02:40:13.20	+04:54:55.4	0.08	19.6
1999er	Joshua	II	10/01/99	02:47:06.88	-02:57:43.9	0.026	19.8
2000eo	Grover	II-n	11/16/00	03:09:08.17	-10:17:55.3	0.010	19.2
2000es	Dr.Teeth	II	11/16/00	04:06:17.87	-03:23:18.2	0.074	19.7
2000fh	Thog	Ia?	11/16/00	04:40:28.66	-05:10:07.7	??	20.1
1999ep	Lua	Ia	09/27/99	04:41:04.76	-03:00:39.6	0.063	19.5
—	Paz	??	03/23/00	08:19:05.51	+02:01:54.9	??	20.8
2000et	Beeker	Ia	11/17/00	08:21:15.21	+01:09:25.3	0.11	19.4
1999ap	Toby Belch	II	02/24/99	08:29:47.4	+04:37:38	0.04	19.4
2000bl	Andacollo	II-P?	03/26/00	08:55:20.44	-07:23:42.9	0.151	19.4
2000bm	Lonco	II-L?	03/23/00	08:58:56.02	+05:10:15.7	??	19.2
1999au	Lucio	Ia	03/09/99	08:58:58.01	-07:22:09.9	0.124	19.2
2000eu	Zoot	Ia	11/16/00	09:00:13.00	-05:35:04.2	0.08	18.7
2000ep	Oscar	II	11/16/00	09:19:49.86	-04:43:28.2	0.024	18.7
1999ar	Abhorson	Ia	03/06/99	09:20:16.00	+00:33:39.6	0.149	19.7
1999aq	William	Ia	03/06/99	09:38:10.8	-05:08:56	0.050	18.8
2000bn	Gabrielito	Ia	03/25/00	09:35:41.15	+04:32:13.3	0.127	18.8
2000bo	Machi	??	03/23/00	09:49:34.92	-03:32:38.3	??	18.2
2000bp	Cuyen	II	03/25/00	09:54:20.63	-04:52:13.3	0.057	19.8
—	Coromandi	II-P?	03/25/00	09:55:51.07	-01:12:48.8	??	20.2
2000R	Cari	II-L	03/23/00	10:01:21.21	-06:33:57.0	0.010	18.9
1999az	Huirol	Ia	02/23/99	10:18:56.4	-10:25:18	0.15	20.5

Table : Cont. SNe candidates from the NGSS survey. Spectroscopic and photometric redshifts are given. Type determinations have been made when possible.

SN	A.K.A	Type	Disc. Date	R.A(2000)	DEC(2000)	z approx.	R mag approx.
1999ba	Hamlet	Ia	02/23/99	10:19:19.4	-02:49:39	0.092	20
1999av	Petruchio	Ia	03/09/99	10:55:49.7	-09:20:23	0.053	18.6
2000cd	Aster	II-n	03/24/00	10:56:48.69	-05:34:40.8	0.047	18.2
2000bq	Ranco	Ia?	03/25/00	11:01:03.24	-05:50:36.2	0.18	20.4
1999aw	Pompey	Ia	03/09/99	11:01:36.37	-06:06:31.6	0.038	17.6
1999bb	Julius Caesar	II	02/23/99	11:05:16.5	-06:01:32	0.180	20.6
2000br	Mario	II	03/25/00	14:03:50.20	-04:01:01.7	0.12	18.8
2000eq	Waldorf	Ia	11/17/00	21:03:57.97	-09:41:31.8	0.174	20.5
2000fi	Scooter	??	11/09/00	21:52:57.14	-06:32:53.9	0.091	18.2
2000fj	Ms_Piggy	??	11/13/00	22:08:52.31	-04:41:39.5	0.088	19
2000fk	Crazy_Harry	??	11/14/00	23:36:26.00	-00:23:17.6	0.149	20.1
2000fl	Cookie_Monster	??	11/18/00	23:46:19.57	-06:31:03.9	0.08	19.8
—	Beauregard	??	??	??	??	0.0591	??
—	Ipanema	??	10/01/99	23:06:45.38	+00:13:08.3	0.055	17.4
—	404	??	03/30/00	??	??	??	??
—	Barkley	??	11/17/00	??	??	0.093	??
—	Bernheim	??	11/16/00	??	??	??	??
—	Cumberland	??	11/09/00	??	??	0.142	??
—	Esteban	??	03/27/00	??	??	??	??
—	Euman	??	03/29/00	??	??	0.069	??
—	Gorge	??	11/14/00	??	??	??	??
—	Gryffindor	??	12/10/98	??	??	0.034	??
—	Laurel	??	03/26/00	??	??	??	??
—	Mancub	??	03/30/00	??	??	??	??
—	Mbu	??	03/27/00	??	??	??	??
—	Rufi	??	03/27/00	??	??	0.1	??
—	Siuyen	??	03/27/00	??	??	??	??
—	Voldemort	??	10/02/99	??	??	??	??
—	Xenia	??	03/30/00	??	??	0.069	??

Chapter 3

Rates of Supernovae in the Local Universe

I present here a Supernova Rate Calculator designed to test the dependencies of the SN rate on a variety of parameters. The rate calculations include an estimate of the luminosity density in the local universe, and a complex control time calculation designed to eliminate any error in the measurement. The control time corrects for the cadence and detection efficiency of the survey, time dilation effects, the variation in SN characteristics, and the galactic and extragalactic extinction. In addition, we discuss preliminary results from direct measures of host galaxy properties and future work in the area. These data will resolve the most influential factors for SN Ia production, further constraining the nature (stars involved, accretion rates, and explosion mechanism) of these systems, and provide critical insights on the robustness of SNe Ia as cosmological tools.

The SNe rate can be expressed using the following equation:

$$R = \frac{\int N_{SN}(z)\,dz}{\int t_{c,tot}(z)(1+z)^{-1}L_B(z)\,dz} \qquad (3.1)$$

where $N_{SN}(\text{z})$ represents the number of supernovae found during the survey, $t_{c,tot}(\text{z})$ is the control time or effective time in which supernovae could have been found for the survey, (1+z) is a time dilation factor associated with the rate of expansion of

space at larger distances, and $L_B(z)$ is the combined luminosity of galaxies within the surveyed region. This rate is typically expressed in units of SNu's. One SNu is equivalent to one supernova per 10^{10} solar luminosities in the R band, per century, or 1 per galaxy, per 100 yrs.

3.1 Number of Events

The integrated number of observed events as the numerator in the rate calculations. To attain this value, we used the SNe yield values for the Nearby Galaxies Supernovae Search Project. Originally, the search located 42 supernovae of various types with 18 type Ia supernovae. As mentioned before, during the resurveying of the data, we found 20 additional supernovae. A type classification for these additional candidates has not been obtained, and many of these objects do not have known redshifts. However, we can use this sample as an upper limit for the rate calculations. We weight the rate based on SNe type using the number of each type found in the NGSS survey.

This portion of the rate calculation remains the largest source of error in the measurement. While this survey was the largest of these campaigns completed at its time, the yield is still rather low. Poisson statistics give us an estimate of our statistical error. For the sample of 18 type Ia events this gives $1/\sqrt{N} \approx 0.236$. Assuming an upper limit of 38 type Ia events, this gives $1/\sqrt{N} \approx 0.162$. Furthermore, our inability to determine the type of the additional 20 events conclusively, which has the potential to double our sample, contributes a large amount of systematic error.

3.2 Control Time

The integrated control time is the third and final component in the rate calculation. In short, this is the effective time that supernovae could have been observed given the conditions of the survey, through the "window" of the survey.

$$t_c = t_c(type, M_R, z, A_R) \tag{3.2}$$

The above equation illustrates that control time depends on the supernova type, the absolute magnitude at peak light, the distance or redshift, and the galactic extinction. The peak luminosity of the event is extremely important. The intrinsic brightness of the objects in our sample dictate the limitations of the survey in depth and in the time we are able to detect the events. In order to determine this factor, both the galactic extinction distance of the object will need to be accounted for.

The supernovae type will effect the shape of the light curve used to calculate the control time for the survey. For SNe Ia, the light curve has a second peak approximately 30 days after maximum light. This allows SNe Ia to be observable for longer periods of time. In order to account for the type of the supernovae, four template light curves were created to correspond with each supernovae type. For SNe Ia, the luminous, branch normal SN 1994D was used. Using a series of polynomial fits to the light curve, the peak absolute magnitude can be approximated by using distributions from previous surveys. For SNe Ia, the peak absolute magnitude was -19.2 $\pm$ 0.6 magnitudes.

Using this information, and the standard relationship between magnitude and distance, an equation can be derived that gives the apparent magnitude of the SN at the time it was observed.

$$R(t, t_e, type, z, A_R) = M_R[t \times (1 + z), t_e, type] + 5log\left(\frac{cz}{H_o}\right) + 25 \qquad (3.3)$$

where the apparent magnitude at observation depends on the time, the explosion date t_e, the supernova type, the distance to the event, and the extinction distribution A_R. A table of peak magnitudes at a certain redshift was created and used in the control time algorithm.

Through the use of the template light curve, it is possible to numerically integrate over all of the possible baselines with which a supernovae of a given peak magnitude could have been detected. The baselines are defined as the difference in time between the template image and the search image and are expressed in days. Both the apparent

magnitude and flux is calculated for each time range. The apparent magnitudes and fluxes are related by the following equations

$$F_T = 10^{-\frac{2}{5}(R_T - Z_{mag})} \tag{3.4}$$

$$F_S = 10^{-\frac{2}{5}(R_S - Z_{mag})} \tag{3.5}$$

$$R_\Delta = Z_{mag} - 2.5 \times log(F_S - F_T) \tag{3.6}$$

where R_T, R_S, F_T, F_S are the apparent magnitudes and fluxes of an event in the template and search images. Here Z_{mag} was assumed to be zero.

The first two equations above relate the fluxes to the calculated apparent magnitudes. The final equation determines the change in magnitude from the calculated template and search image fluxes. With the apparent magnitudes, it is now possible to calculate the probability of detection for each Δ t value. The probability is given by the following equation

$$\epsilon(R, cond.) = \frac{T(cond.)}{1 + e^{\frac{R - R_c(cond.)}{S(cond.)}}} \tag{3.7}$$

where T(cond.) is the maximum efficiency possible for the condition rank, R_c is the limiting magnitude, and S(cond.) controls the shape of the roll-off for the light curve. The condition rank was a quality rating 1 to 3 assigned to each frame based on the condition of the subtraction and the seeing conditions on when the image was taken. Each quality ranking corresponds to a different set of maximum efficiency values, limiting magnitudes, and shape variables. For a condition of 1, T = 0.949, S = 0.979, and R_c = 20.718. For a condition of 2, T = 0.801, S = 0.450, and R_c = 20.316. For a condition of 3, T = 0.656, S = 0.384, and R_c = 20.552.

The effective control time can now be expressed as the sum of the probabilities for every possible Δt value

$$t_c = \sum P(t_e) \Delta t \tag{3.8}$$

where P(t_e) is the efficiency calculated from equation (3.7), and Δt is the time change between the template and search images.

This makes up the bulk of the control time calculations. However, there are several parameters such as the peak magnitude that have yet to be explained. As stated before, the peak magnitude depends on a variety of factors including the type of the supernovae and the extinction from the host galaxy. Each supernovae type has a distinctive absolute magnitude distribution. These have previously been published. The distributions can be used to numerically integrate over a range in possible peak magnitudes. The range used in our calculations was from -16 to -22 mag.

The magnitudes then had to be corrected for extinction. While the survey attempted to limit Galactic extinction by searching outside of the Galactic plane, host galaxy extinction intrinsic to the environment of the event has a large effect on the detection efficiency. We assumed an intrinsic distribution of extinctions similar to one used in a paper by Jha et al. (1999). They used Monte Carlo models to predict the amount of extinction experienced by an object at any location in the galaxy. These models calculated the extinction in the V-band. Therefore, it was necessary to correct this for the R-band. To do this, we had to use a variety of other assumptions. Among these was the assumption that dust grains have cross sections on the order of the wavelength of light. This allowed us to assume that scattering was proportional to this wavelength. In addition we assumed that the ratio of extinction in V to B - V color excess was nearly the canonical value of 3.1. After combining this information with the Monte Carlo model, we arrive at an equation for the probability of extinction.

$$P(A_R) = Ce^{\frac{-(A_R - \bar{A})}{S_A}} \tag{3.9}$$

where $\bar{A}$ and S_A are parameters for the best-fit. The constant C is a proportionality constant found by normalizing the extinction probability function. The model we used gives values of C = 2.722, $\bar{A}$ = -0.2355, and S_A = 0.347.

The extinction probabilities calculated in this way were then used in the control time calculations to determine the magnitudes. This extinction probability distribution is only correct for Type Ia supernovae. This type occurs most often in elliptical galaxies which have small amounts of dust and, therefore, a lower amount of extinction.

Finally, we were able to determine the overall control time. This can be expressed as the integral sum of control times multiplied by all reasonable absolute magnitude and extinction probabilities.

$$t_{c,tot,z} = \int \left[\int t_c(type, M_R, z, A_R) P(M_R) dM_R \right] P(A_R) dA_R \qquad (3.10)$$

Here the probability is a function that is dependent on SNe type, peak magnitude, redshift and extinction. This gives the total control time when calculated for all redshifts within the search range, and for all baselines. A plot of this probability distribution shows the behavior of the control time as a function of redshift (Figure 3.2).

At lower redshifts, it is much easier to detect SNe because of the lower levels of extinction, and the higher apparent magnitudes. As depth increases, the control time calculations become the limiting factor in the SNe rates.

3.3   Weighted Rates

A rate expressed as the number of events per a unit time gives no indication of the volume of amount of material. To successfully compare rate results from different surveys, there must be a component of the rate that constrains the survey coverage. The rate can be scaled by an assumed volume projected outward over the field of view of the survey. The maximum distance is dictated by the limiting magnitude of the survey. The rate can also be weighted by an estimate of the total number of stars surveyed. This luminosity density relies on the distribution and brightness of galaxies in the local universe. Here we discuss both methods.
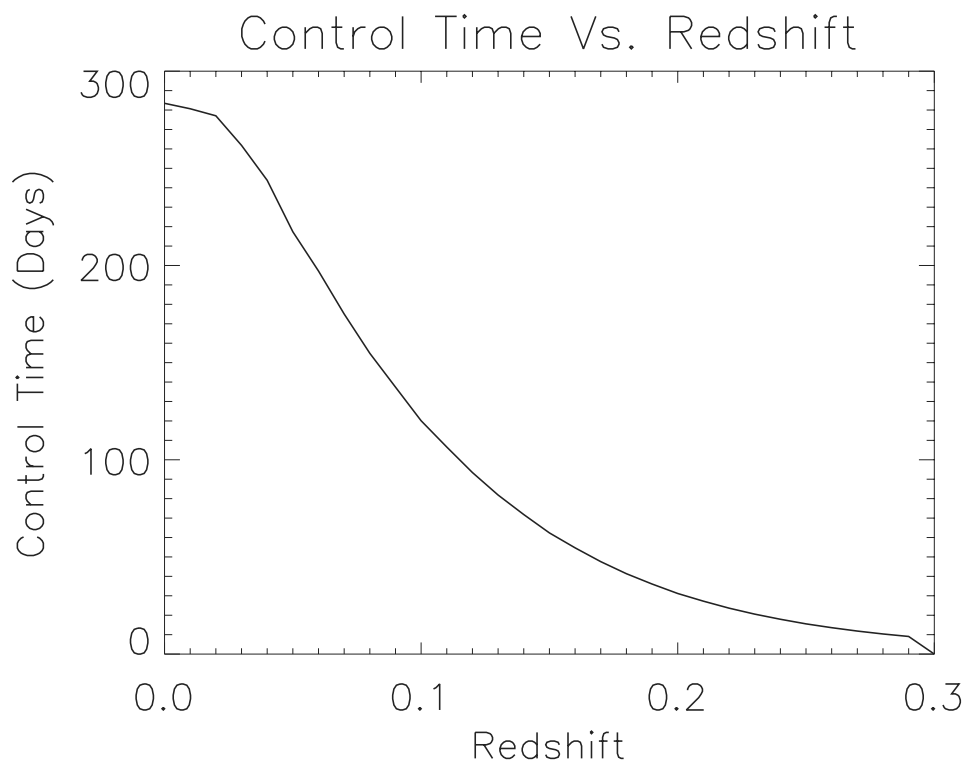
Figure 3.1: The control time is the effective time for the survey. Shown is the calculated probability distribution as a function of redshift. The control time limits our ability to detect SNe at larger redshifts.

40

3.3.1 Volume Weighted Rates

Volume weighted rates give an effective spacial extent for the survey. The survey covers ~ 500 square degrees of sky. The survey depth is limited to a redshift of 0.3. These serve as the bounds for the survey volume. If we are assuming "wedges", the arcelength is defined by $s = \theta d$. The surface area is defined by the solid angle by $A = \theta^2 d^2 = \Omega d^2$. The volume enclosed is basically the length x area, so $V = Ad = \Omega d^3$.

Cosmologically speaking, the volume is the integrated comoving volume defined by the proper motion distance (or the actual distance). The relationship between this actual distance and the luminosity distance is given by:

$$\frac{d_L}{(1+z)} = d_m \tag{3.11}$$

The proper motion distance, d_m, is defined in term of redshift by the dynamic constituents of the universe,Ω_M, Ω_Λ, Ω_K, and H_0, in the equation

$$d_m = \frac{c}{H_0} \int_0^z \left[(1+z)^2(1 + \Omega_M z) - z(2+z)\Omega_\Lambda \right]^{(-1/2)} dz \tag{3.12}$$

To estimate this, we will use the concordance model parameters.

H_0	71 km/s/Mpc
Ω_M	0.27
Ω_Λ	0.73
Ω_K	0

Throughout this paper a dimensionless Hubble constant $h = 0.7$ will be assumed. Doing this, we get a rate of $R = 0.414 \, h_{70}^2 \times 10^{-4} \text{ Mpc}^{-3}$.

3.3.2 Rates Weighted by Luminosity Density

The luminosity density is the luminosity of all galaxies at a specific redshift in the field of view our survey. This function consists of an analytical expression for the density of galaxies as a function of redshift. To get the total luminosity volume for

the survey, the luminosity density function is multiplied by the volume and integrated over our range in redshift.

$$L_B(z) = \int \mathcal{L}_B(z) dV(z, \Omega) \tag{3.13}$$

Here, $L_B(z)$ is the luminosity of the region and V is the volume. The conic volume for the area surveyed was calculated using Hubble's Law and assuming that all candidates were within the Hubble flow and were located at low redshifts. The solid angle per pointing$\Omega \approx 0.9$ square degrees as used. We then used the total control time for each baseline to give the total effective solid angle

$$V = \Omega \frac{c^2 z^2}{H_o^3} \tag{3.14}$$

The luminosity density function we used in our rate calculations was derived from the results of several galaxy redshift surveys and the work on an integrated luminosity function of Lilly et al. (1995). This gives a function for total galaxy luminosity assuming a guassian fit where $\alpha = 1.9 \pm 0.1$ and the luminosity is approximately 0.4 ± 0.2 $L_\odot$.

$$\mathcal{L}_B(z) = (2.0 \pm 0.4) \times (1 + x)^{1.9 \pm 0.5} \times 10^8 h L_\odot Mpc^{-3} \tag{3.15}$$

When this function is multiplied by the volume described above and integrated over the range in redshifts, the following expression is derived for the total luminosity in the survey volume.

$$L_B(z) = \int_{0.0}^{0.3} (2.0 \pm 0.4) \times (1 + z)^{1.9 \pm 0.5} \times 10^8 h L_\odot Mpc^{-3} \times \Omega \frac{c^3 z^2}{H_o^3} dz \tag{3.16}$$

where h = 0.7, $H_o =$ h 100km/s/Mpc, Ω is the solid angle, and c is the speed of light.

Figure 3.1 gives the integrated luminosity density as a function of redshift. It is clear that the luminosity density is the limiting factor in the rate calculations at lower redshifts. In the local universe, the density of galaxies is low and increases with the depth of the survey.

To determine the total luminosity within the volume of the fields surveyed, we assumed that the luminosity could be integrated over all redshifts to give the total luminosity in the region. However, this lies on a basic assumption that the luminosity density is constant over all redshift bins. This is a false assumption. In order to fix this error, our code needed to be rearranged to integrate over redshift bins as shown below.

$$L_B(z) = \int_{z-dz/2}^{z+dz/2} \mathcal{L}_B(z) dV(z) \qquad (3.17)$$

Through the use of this equation, we can assume that the luminosity density is constant within the given range of redshifts as long as the bins are small. Therefore, it can be factored out of the integral. The volume portion of the integral can now be rewritten to be the change in volume for a given redshift bin as shown below.

$$L_B(z) \simeq \mathcal{L}_B(z) \left[V(z + \frac{dz}{2}) - V(z - \frac{dz}{2}) \right] \qquad (3.18)$$

The function of luminosity density of galaxies at a given redshift was described in equation (3.14). As stated before, the second portion of this equation describes the volume while the first half describes the luminosity function of galaxies in the local universe. This was derived from the work of Lilly et al. This methods produces a rate of $0.220 \, century^{-1} [10^{10} L_{sol}(B)]^{-1}$ in the B-band.

In an effort to make the rate calculations as accurate as possible, we examined recent corrections to these and similar luminosity density functions. The work of Dahlen et al. (2005) published luminosity densities derived from semi-analytical fits to data provided by other authors. These fits post-date the Lilly et al. fits by a
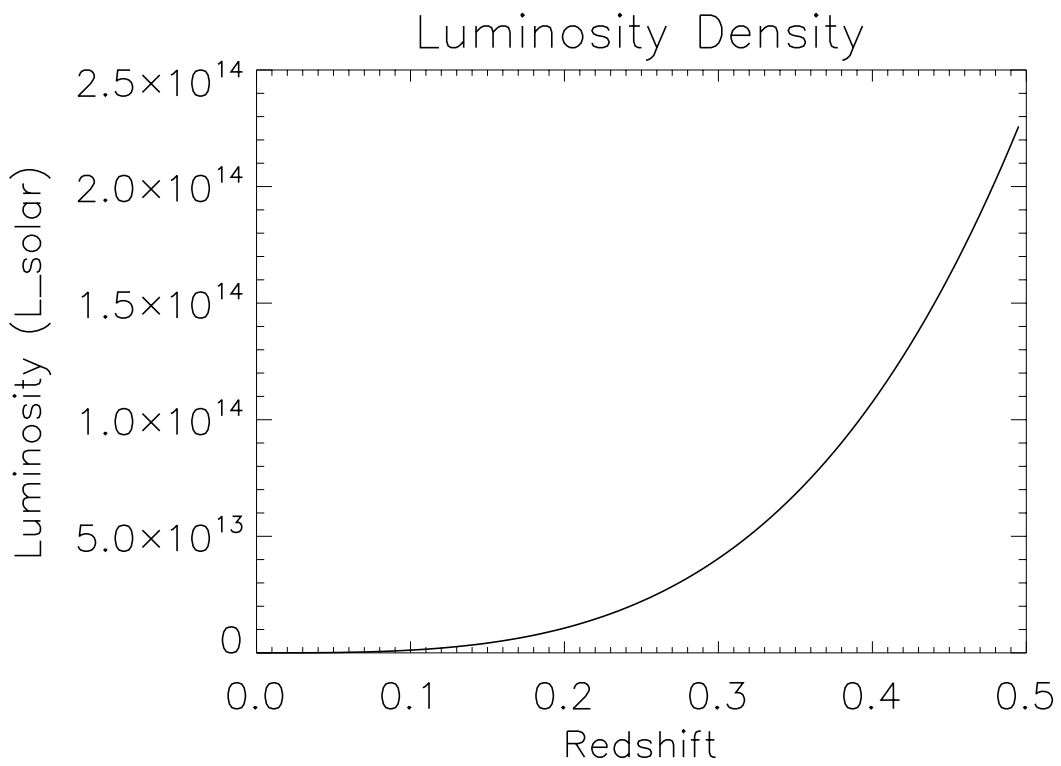
Figure 3.2: Plot of the luminosity density as a function of redshift. The Luminosity density serves to place a lower limit on the integrated rate calculations.

decade.

Several problems arose when we tried to convert Dahlen's work to fit our code. First, they give luminosity densities in units of erg s^{-1} Hz^{-1} h$_{70}$ Mpc^{-3}. One benefit of this alternative approach is a dependence of the luminosity density functions on a wavelength regime. This allowed us differentiate the calculated supernovae rate in different optical bands. First, however, we needed to convert from erg s^{-1} to solar units.

$$\rho \Rightarrow \mathrm{erg\,s^{-1}\,Hz^{-1}\,h_{70}\,Mpc^{-3}} \tag{3.19}$$

The luminosity density (ρ) is given in a log scale. The conversion is defined by

$$\mathcal{L}_B(z) \equiv \int_B \rho d\nu \tag{3.20}$$

where the luminosity density function ρ is integrated over the effective bandwidth of the passband. For the B-band, the bandwidth is approximately 3500 Å to 5500 Å. For the R band, the bandwidth increases to approximately 5500 Å to 7500 Å. For the K band, the bandwidth is in the range of 1.95 μm to 2.5μm.

In the initial calculations of the luminosity density, the R-band was used. Here we do the same and assume that this will result in the most accurate value. Using values obtained using the above definition, we can now derive an equation for luminosity density in units of solar luminosity and volume using the following relation,

$$\mathcal{L}_B(z) = \frac{1}{L_\odot}\rho(z,\nu)\Delta\nu\Delta V(z) \tag{3.21}$$

We can convert to solar luminosities from erg/s with the relation L$_\odot$ = 3.84 × 10^{33} erg/s. This function can then be put into our luminosity function in the place of the old $\mathcal{L}_B$(z) function.

Using this new luminosity function in the rate calculation resulted in a rate per luminosity that was slightly higher than our original function while still in line with

other low-z rate results.

$B-$**band**

The Dahlen et al. (2005) luminosity densities are semi-analytical fits to data provided by other authors, and data from the GOODS project. Dahlen's work allows for weights to the different colors of light. This may provide a better tracer for the total number of stars or total number of progenitor stars for different SNe types.

Using this method, we get $R = 0.272\,h_{70}$ SNe per century per $10^{10}\ L_{B,\odot}$. Tomas Dahlen's luminosity density function is lower than our previously calculated rate, resulting in a higher overall luminosity weighted event rate.

$R-$**band**

The same methods can be applied to the $R-$band, assuming this better tracks the number of stars than $B-$band light. Here,

$$\mathcal{L}_R(z) \equiv \int_R \rho_R\, d\nu \tag{3.22}$$

In the approximate range of 5500Å to 7500Å. Here we get $R = 0.131\,h_{70}$ SNe per century per $10^{10}\ L_{R,\odot}$.

$K-$**band**

There are plenty of arguments for the $K-$band being a good tracer of total stellar mass surveyed (cf. Mannucci et al. 2005), although there could be thermal dust light there too. Nonetheless, using the approximate range of $1.95\mu m$ to $2.5\mu m$ for the $K-$band, we get $R = 0.178\,h_{70}$ SNe per century per $10^{10}\ L_{K,\odot}$

Chapter 4

Results and Discussion

Using the sample of 17 photometrically and spectroscopically confirmed SNe Ia, we an place a lower limit on our SNe rate calculations. Figure 4.1 provides the cumulative rate of supernovae in relation to the observed distribution of SNe at a given redshift. We calculate a volumetric rate of $0.414 \times 10^{-4} yr^{-1} Mpc^{-3}$. We obtain a SNu rate using binned wavelengths of $0.272 \, century^{-1} [10^{10} L_{sol}(B)]^{-1}$ in the B-band, $0.131 \, century^{-1} [10^{10} L_{sol}(B)]^{-1}$ in the R-band, and $0.178 \, century^{-1} [10^{10} L_{sol}(B)]^{-1}$ in the K-band. The non-binned SNu rate gives $0.220 \, century^{-1} [10^{10} L_{sol}(B)]^{-1}$ in the B-band. Our calculated volumetric rates agree well with the luminosity density rates. In bluer passbands, most of the flux can be attributed to young, massive, hot stars. These stars have vary short lifetimes and this population serves as a good tracer for the star formation rate (SFR). The higher rates in the B-band point towards a dependence on the SNe Ia rates on the SFR. These rates are in concordance with other SNe rate calculations in similar redshift regimes. Recent rate studies give values for the rates in late type spirals to be 0.88 SNu for type II, 0.16 SNu for type Ib/c, and 0.24 SNu for type Ia (Cappellaro et al. 1997).

From Figure 4.1, it is apparent that the calculated rate under predicts the observed number distribution, especially at higher redshifts. This is largely a result of the extinction distribution chosen. For these rates, we used an extinction curve described by exponential decay with the peak located at 0.0. If the extinction distribution is moderately adjusted such that $< A_V > = 1.0$, and renormalized, we get the
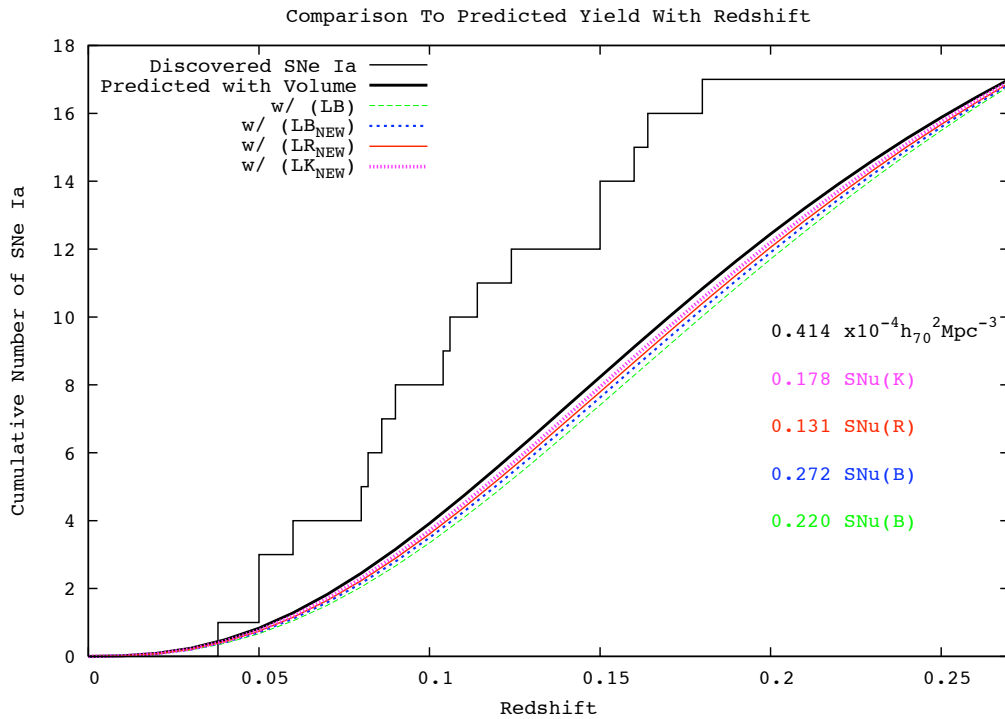
Figure 4.1: Rate results, with the redshift distribution of observed SNe Ia outpacing predicted distributions from the volume surveyed (black line), and the total galaxy luminosity surveyed in the blue and near-infrared passbands (Wolff et al. 2010, in prep).
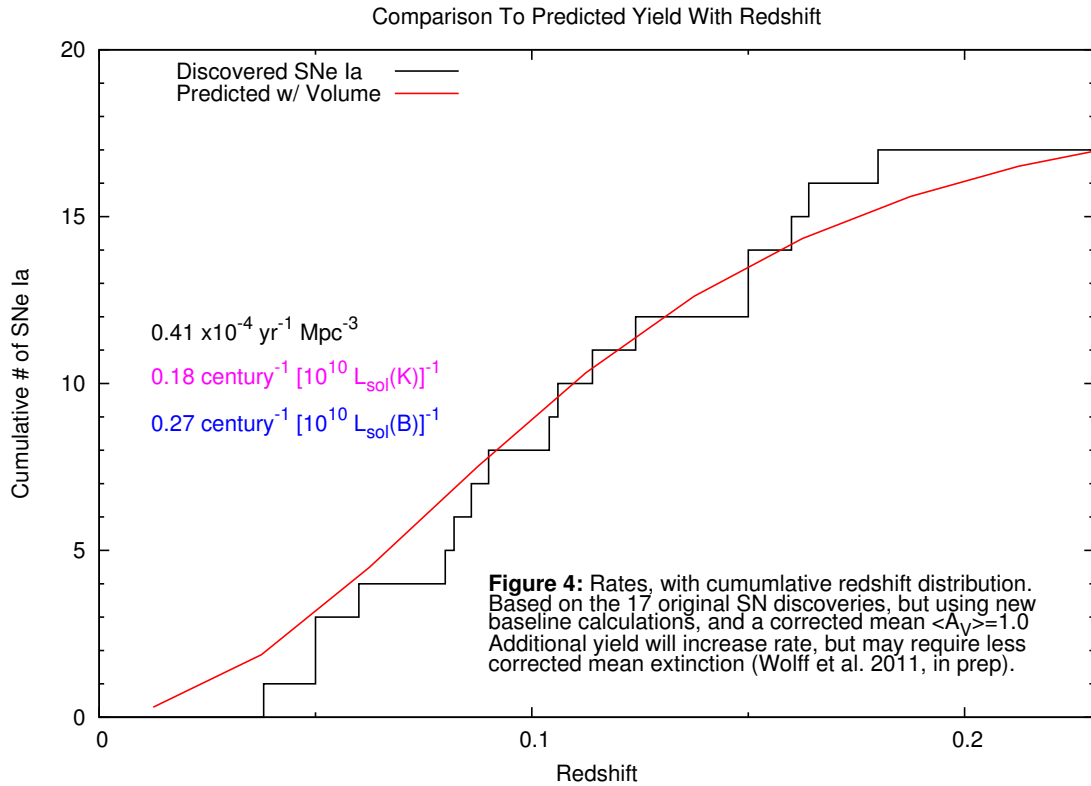
Figure 4.2: Rates, with the cumulative redshift distribution. Based on the 17 original SN discoveries, but using new baseline calculations, and a corrected mean $< A_V >= 1.0$. Additional yield will increase rate, but may require less corrected mean extinction (Wolff et al. 2011, in prep).

49

distribution seen in Figure 4.2. The change in the rate resulting from this amount of extinction is negligible, however, the kludge is not physical.

Although the model now seems to favor the observed distribution, it slightly over predicts the observed distribution at lower redshifts and slightly under predicts the numbers at higher redshifts. There could be a variety of possible causes for this, for example, the error in the observed number of SNe Ia and their redshifts. However, an inherent overproduction of SN Ia per unit mass would also account for this discrepancy. This would indicate a secondary enhancement of the rate, such as the rate of star formation, indicating that massive short-lived stars are tied to these events. A delay in the rate of SNe Ia from the rate of star formation would also explain the difference, indicating that low-mass long-lived stars are tied to these events. Lastly, the extinction distribution was chosen somewhat arbitrarily and is not completely physical. In order to test the effects on the uncertainty in the observed number of events and on the extinction distribution, we conduct a preliminary parameter study.

Discrepancies between our rate results and those in the literature led us to reconsider the extinction distribution used. The extinction distributions are not incredibly well understood. We have assumed an extinction distribution that is drawn from models of various line of sight extinctions in spirals with different inclinations, and with observations of the extinctions of SNe Ia from cosmological studies. However, the last is inherently biased against heavily extincted events, as those are unseen (or typical not coveted). We can solve for the extinction distribution using either a Markov Chain or minimum χ^2 testing.

For convenience, we'll assume the functionality of the extinction distribution is Gaussian, characterized by a mean of $\bar{A}_R$ and a variance of σ_A^2. Here, $\bar{A}_R = \{-10...10\}$ and $\sigma_A^2 = \{0...10\}$, and the function is truncated below zero. The rate equation can be re-written as:

$$R \times [t'_c(z_i)\,\Delta V(z_i)] = N(z_i) \tag{4.1}$$

Where the left-hand side shows the calculated number of SNe in the ith redshift bin,

and the right-hand side is the observed number of SNe in that same bin. We make the cumulative distributions by:

$$\sum_{(i=0)}^{n} R \times [t'_c(z_i) \, \Delta V(z_i)] = \sum_{(i=0)}^{n} N(z_i) \tag{4.2}$$

For an assumed $\bar{A}_R$ & σ_A, determine:

$$\chi^2 = \sum_{(n=0)}^{k} \frac{(O_n - E_n)^2}{E_n} \tag{4.3}$$

Where n is the integrated redshift bin. We probe the full grid of parameter space, asking if $\chi_i^2 < \chi_{min}^2$. This same test should also be done as a MCMC to see if a solution can be found faster.

The only obstacle we have still to overcome involving the control time concerns the few declining supernovae that we discovered in our survey. The code we wrote only accounts for magnitude differences between the template in search images that are positive. Thus, the small number of declining supernovae that were discovered are serving to subtract from our overall control time. It is our aim to adjust the code in future works so that both risers and decliners are taken into considered within the calculations.

Figure 4.3 gives an example of for this type of parameter study. To test the error in the number of events used, we test three possibilities. As the spectroscopic type and redshifts determinations are very well understood, we use these 15 SNe Ia as the lower limit to our sample. A sample of the 17 SNe Ia with photometric or spectroscopic type and redshift information was used as the middle estimate. To obtain an upper limit, we include all of the objects with unknown type information in the rate calculations which gives 38 SNe Ia. Three or more models for the extinction distribution can be tested. The first model used the originally assumed probability distribution described by an exponential decay with a peak at 0.0. For the other probability distributions, a Gaussian curve truncated at 0.0 was assumed. We test reasonable peaks in the Gaussian at 1.0 and 2.0.

The rate model will increase with both the number of SNe events used in the calculations and with the average value in the extinction distribution. From Figure 4.3 it is clear that the rate model continues to under predict the observed distribution even at reasonable upper limits. This implies that the stellar death rate lags behind the density of stellar objects. Otherwise stated, the rate of SNe production lags behind the star formation rate. This agrees with rate trends observed at higher redshifts (Figure 4.4). These results serve as further evidence that the SNe Ia rate is limited by either a Time-dilation Model requiring an extended development time for the SNe Ia progenitor system or by a Metallicity model that describes a notable effect on the production efficiencies with higher metallicities. Testing the effects on SNe Ia production of host galaxy properties such as the star formation rate (SFR), metallicity, and stellar population ages will help to constrain these effects.

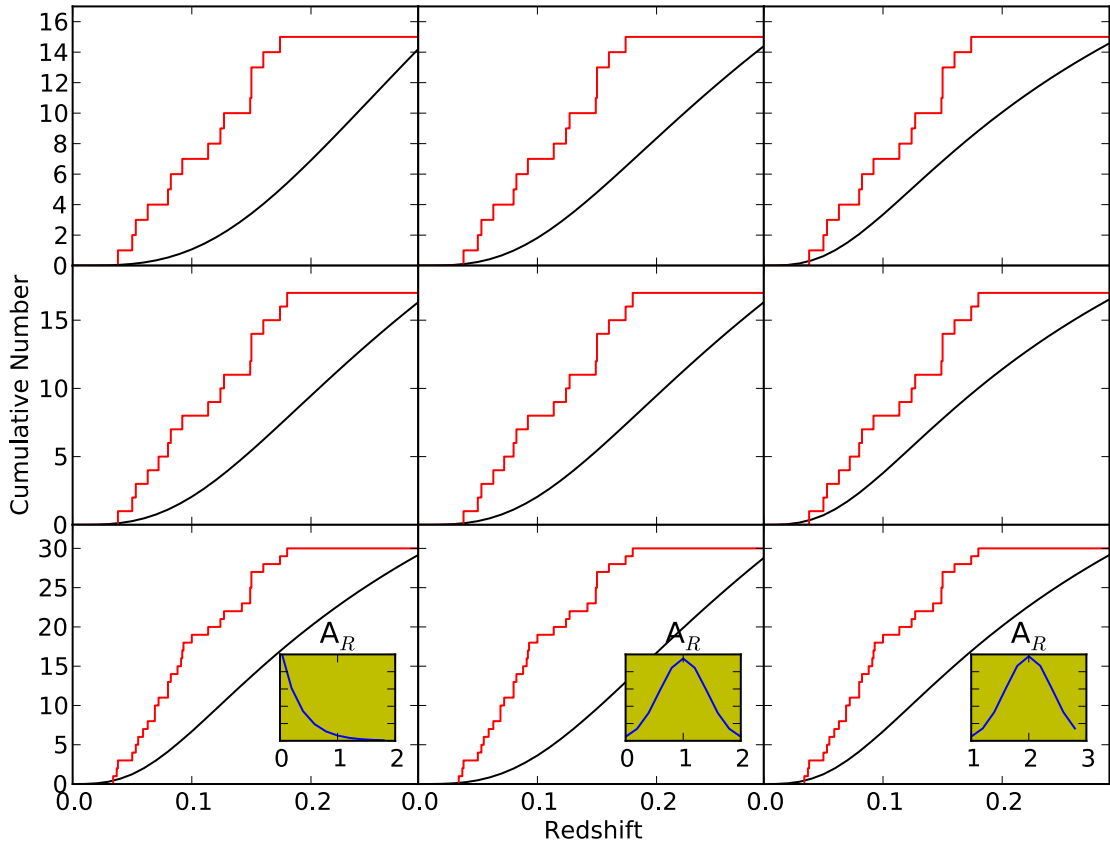Figure 4.3: This plot illustrates a parameter study designed to test the effects of uncertainties in the observed number of SNe and the extinction models. SNe number of 15, 17, and 38 events were used on the vertical axis. Three extinction distributions were tested along the horizontal axis as displayed in the lower right corners. It is clear that the rate increases with both the average extinction and the number of events.
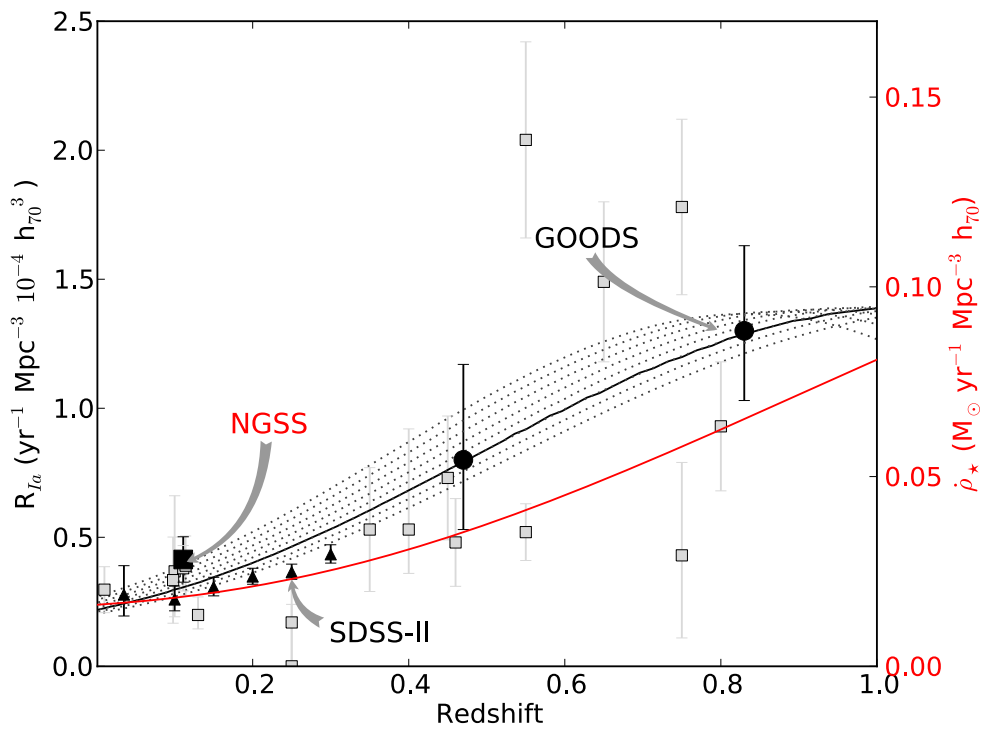
Figure 4.4: SN Rate evolving with redshift. Both a normal (red) and time-dilation model (black with confidence intervals) are shown. The NGSS rate agrees with low-redshift rates from SDSS. These rates will be compared to high redshift results from the GOODS survey and others to test the rate evolution models.

Chapter 5

Future Work

5.1 Motivation

As discrepancies in predicted distributions continue, it is important to address the effects of ages, metallicities, or star-formation rates on SN Ia production. Direct measures from the relatively small sample of SN Ia hosts (≈ 60) from the Nearby Galaxies Supernova Search project (1998-2001; Strolger 2003) may provide more leverage than the current convention of indirect measures on large host samples. We calculate the low-z SN Ia rate, weight the calculations by properties of their hosts (such as metallicity, rate of formation of new stars, and the total stel- lar mass), and draw conclusions based on comparisons to the same properties in galaxies that do not host SNe Ia. The hope is to determine if metallicity has any impact on SN Ia production, which has implications on the robustness of these tools for precision cosmology. It also sheds light on the mysterious progenitors of SNe Ia, the stars that are involved, and the detailed physical mechanisms used to result in a SN Ia event which still remains unresolved.

Previous SN Ia rate trends with environmental parameters have been largely ambiguous, due to large variance in indirect proxies for galaxy parameters (i.e., colors, luminosities, and Hubble types), and limited sample sizes. More recent studies of large low-z SN samples (i.e., SDSS, LOSS, & SNLS) have recently focused on SN Ia luminosity trends with host properties, exploring more trustworthy proxies for galaxy
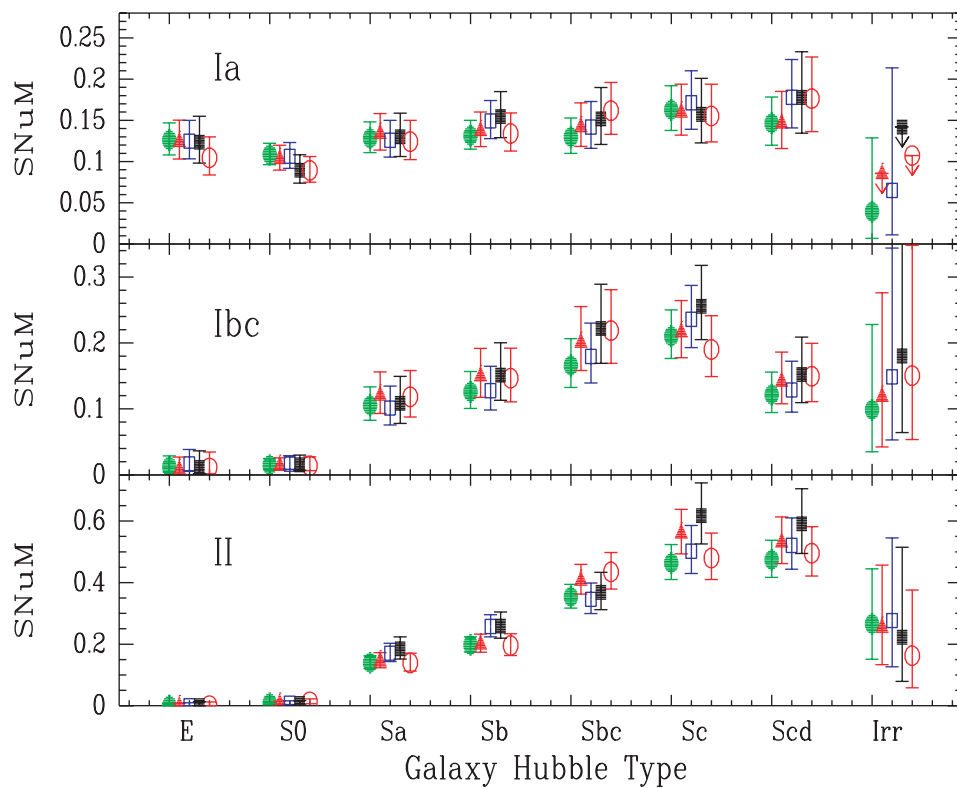
Figure 5.1: The SN rates (for a galaxy of the fiducial size) from different SN samples. Previous measurements have been ambiguous and are subject to large uncertainties. Solid dots: the full sample (total number of SNe = 929). (Li et al. 2011)

SFRs, ages, metallicities, and total stellar masses through full-spectrum stellar population fits, and luminosity-metallicity relations. (e.g., Brandt et al. 2010, Maoz et al. 2010, Strolger et al. 2010), but all have been limited by simplifying assumptions on the ages and star formation histories of the parent sample, and none have evaluated metallicity's impact on SN Ia production.

While these investigations are furthered by ample host sample sizes (≥ 100 each), they remain limited by the known variances in the indirect proxies for galaxy characteristics (i.e., mass-metallicity, Tremonti et al. 2004), the lack of SFR and metallicity information in broad SED fits (e.g., Sullivan et al. 2010), and the quality of the spectra obtained for full spectrum analysis (e.g., Brandt et al. 2010). For example, in the case of the recent SDSS and LOSS analyses (Brandt, et al. 2010, Maoz et al. 2010), their $r'_{\mathrm{lim}} \leq 18.2$ galaxies at $z \sim 0.1$ have only S/N ~ 15 per Å, at R ~ 2000.

We ultimately seek to improve the measure of galaxy properties for a complete sample of SN Ia host galaxies from the NGSS project. Comparisons will be made to both direct and indirect metallicity/age results from the literature (e.g., Gallagher et al. 2008, Sullivan et al. 2010, Brandt et al. 2010), and other pending results from various supernova surveys in several redshift regimes, including the GOODS/HST-SN surveys (Strolger et al. 2010).

5.2 Preliminary Results

The SN sample produced by the NGSS project was statistically robust and allowed us to begin investigating the host galaxy environments. We have run a four semester campaign with an average of 6 nights a semester to obtain spectra for the host galaxies of ≈ 40 of our original sample ($\langle z \rangle = 0.11$). We used the KPNO 4.0-meter telescope with the Raleigh Creighton Spectrograph and the Hale 200-in Telescope with the Double Spectrograph. We had a wide spectral coverage from ~ 3500Å to 8500Å. These data have been used to conduct a census of environments for a sample of low redshifts galaxies, matching to Vazdekis MILES SSP models via cross-correlation and least-square fits to constrain the ages and metallicities of host in our sample. Our present methods for determining the ages and metallicities of our sample of ~ 60 host
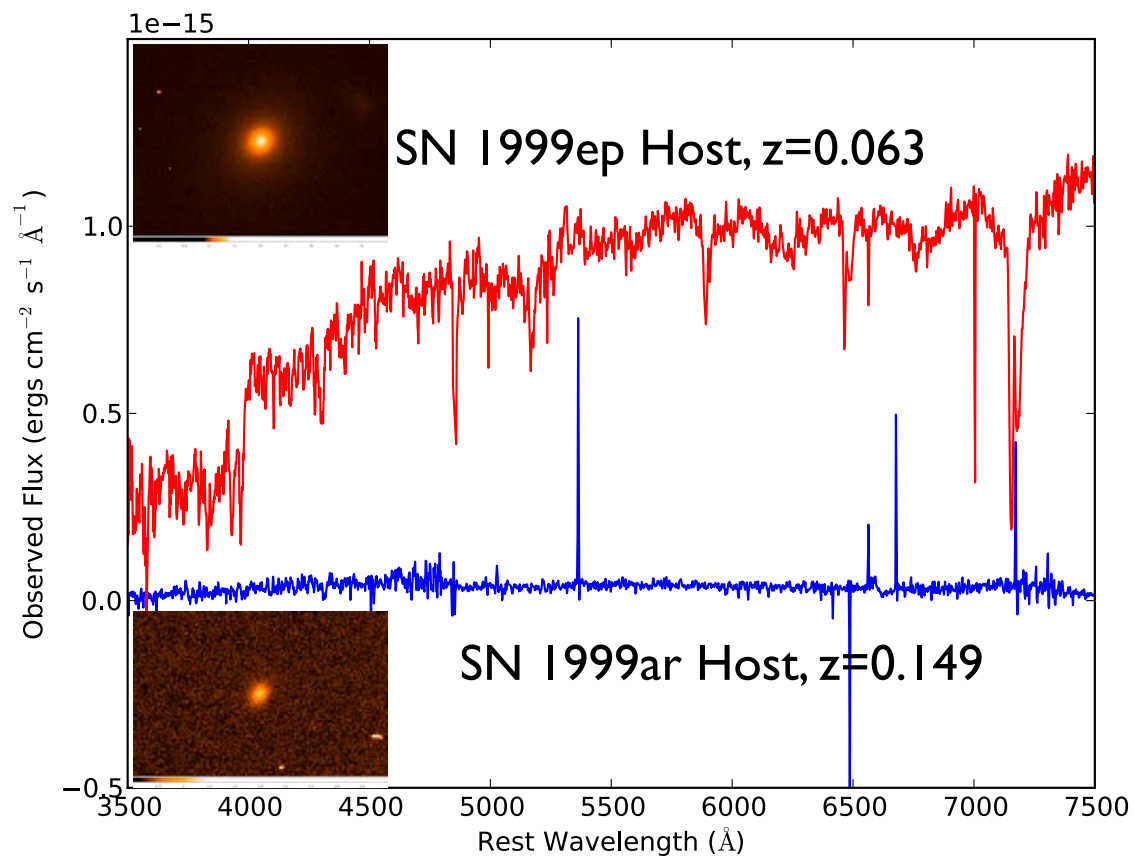
Figure 5.2: The NGSS host galaxy is an early-type elliptical, yet the host for SN 1999ar clearly shows nebular lines indicative of star formation.

galaxies is a self-written code that successfully measures the square of the difference between each of the spectra and all 304 combinations of age and metallicity available in the Vazdekis' library. The code reports the model producing the least square fit as a most likely fit. We do not anticipate issues regarding active versus passive galaxies. When emission lines are present, we will use Hα (relative to Hβ) to measure the rate of star formation in these galaxies (Kennicutt 1992). Gas-phase metallicity will be measured via the R$_{23}$ method (Pagel et al. 1979) from [OII] and [OIII] and via the N2 method (Denicolo, Terlevich & Terlevich 2002) from Hα and [NII] (e.g., Kudritzki et al. 2008, Kewley & Ellison 2008). The sample provides a validity test for the mostly indirect trends being established for SNe Ia from the LOSS, SDSS, SNfactory and other surveys, and ultimately steer future investigations towards more precise SN Ia cosmology.

We have obtained $\sim \frac{2}{3}$ of our host galaxy sample and fully analyzed about 10 hosts. Preliminary results can be seen in Figure 5.3. The hosts seem to be older with higher metallicities. This does not directly imply that galaxies must be older with higher metallicities to host SNe Ia. However, it does support the Delay-time Limit (Strolger et al. 2010), which supports an older population, and the Metallicity Limit (Koybayashi et al. 1998), which supports a more metal-rich environment. We anticipate reducing and constraining errors on the measurements in future works. This result represents only a small subset of our entire dataset. At seven our of 60 host galaxies, we are far from being able to establish trends for SNe Ia production. However, as we complete our sample, we are getting closer to constraining the environments that yield these important and poorly understood cosmological tools.
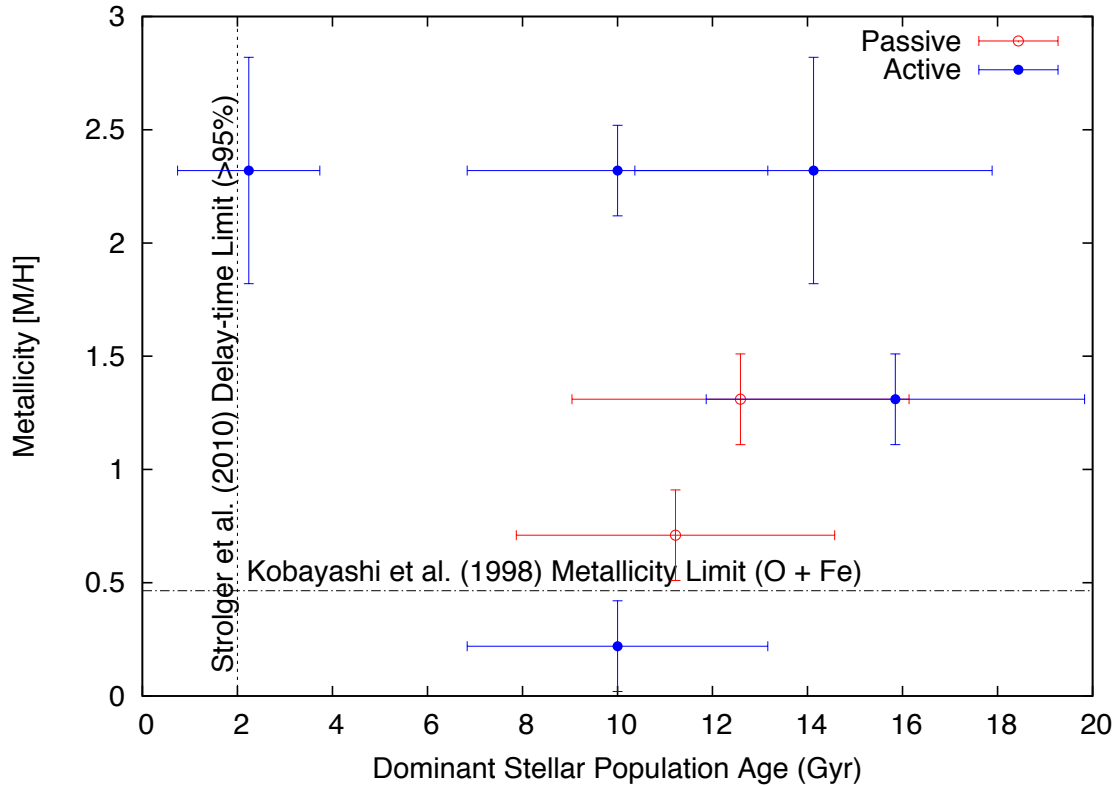
Figure 5.3: Scatter plot depicting the preliminary results from this project. Notice the tendency towards higher metallicity and higher age. Delay-time Limit: Progenitor system depends on White Dwarf accreting mass from a neighboring star. WD production is on the order of millions of years. With other factors we don't expect SNe Ia to the left of the vertical line. Metallicity Limit: SNe Ia can only be found in the environments where the timescale of metal enrichment is short. If the iron abundance it too low, the stellar wind will be too weak for SNe Ia to form.

Appendix A

Supernova Rate Calculator

The Supernova rate calculator constructed for this project consisted of a variety of algorithms produced in IDL. The figure below provides the structure for the program. The subsequent figures provide the code for each routine.
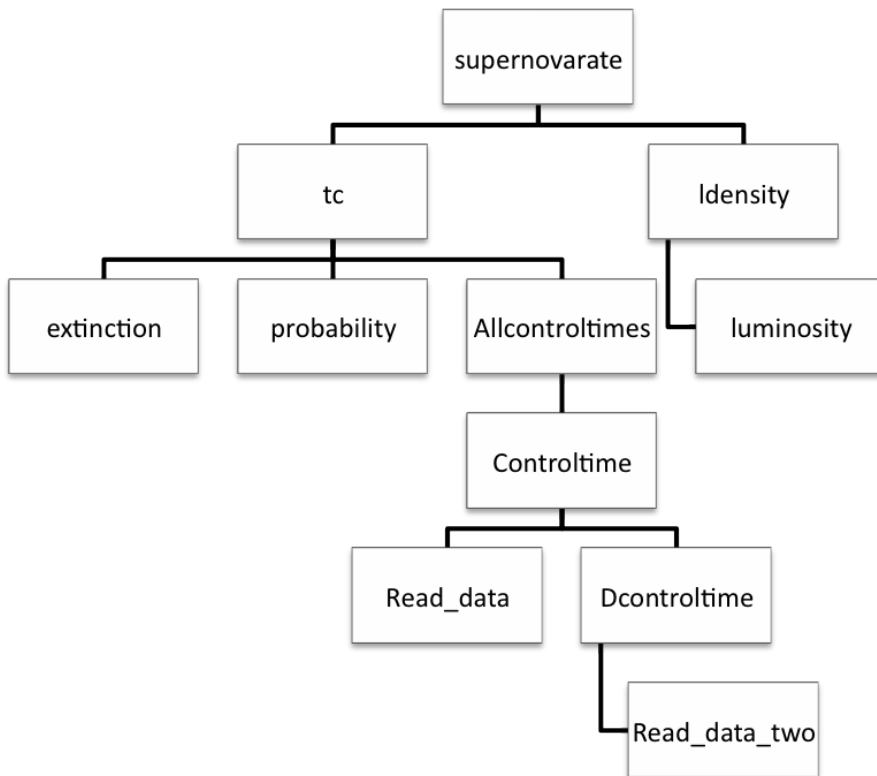
Figure A.1: Shown is the logical hierarchy for the supernova rate calculator algorithm. All of this project was written in IDL.

```
                          supernovarate.pro

Pro SupernovaRate, Rate

!EXCEPT=0
Number = 18
ze=0.
sum=0.

;open a file for writing
filename='/Users/schuylerwolff/SGCODE_B/snroutput.txt'
openw,25,filename

while ze LT 0.3 DO BEGIN
  if (ze eq 0) then begin
    ld=ldensity(0,0.001)
    ;v=0
    ct=tc(0.001)
    sum=sum+ct*ld*0.01
  endif else begin
    ct=tc(ze)
    ld=ldensity(0,ze)
    ;v=volume(ze,0.01)
    sum=sum+((ct*ld))/(1+ze)*0.01
        endelse
  printf,25,ze,ct,ld
  ze=ze+0.01

END
```

Figure A.2: The supernovarate.pro algorithm. This program is responsible for numerically integrating all portions of the rate calculation over the redshifts available in the NGSS survey.

```
                              tc.pro

Function tc, z

SUMA=0
exta=0
step=0.5

WHILE exta LT 3 DO BEGIN
   sum=0
   mag=-22
   maxmag=-16

   WHILE mag LT maxmag DO BEGIN
      value= allcontroltimes(z, mag, exta)*probability(mag)*extinction
(exta)*step
      sum=sum+value
                 print, mag, allcontroltimes
(z,mag,exta),exta,probability(mag),value
      mag=mag+step
   END


   suma=suma+sum*step
   exta=exta+step
END

return, suma

END
```

Figure A.3: The tc.pro algorithm. This program is responsible for a calculation of the total control time at a given redshift. It calls three subroutines responsible for calculating probabilities for the extinction, peak magnitude, and type of the SNe.

```
                        allcontroltimes.pro

FUNCTION allcontroltimes,z,mag,exta

filename='/Volumes/iDisk/Public/SGCODE_B/deltattable.txt'
sumtc=0
i=0

OPENR, 1, filename
data = fltarr(3,165)
readf, 1, data
close, 1

WHILE i LT 165 DO BEGIN
    sumtc=sumtc+data[2,i]*controltime(z,mag,exta,data[0,i],data[1,i])
    quality=data[1,i]
    i=i+1
END

return, sumtc

END
```

Figure A.4: The allcontroltimes.pro algorithm. This program is designed to account of the possible spread in the baselines of the search, or the time between the Search and Template epochs.

*

<pre>
                        controltime.pro

FUNCTION controltime, z, mag, exta,DeltaT,quality

count = 610.
tc = 0.
s = 0.45
;DeltaT = 277

filename='/Volumes/iDisk/Public/SGCODE_B/94D_smooth.txt'
read_data,data,filename
;print, data

peakmag = dcontroltime(z)
stretch=(mag+19.5+0.6)/0.6
peakmag=peakmag+(-19.5-mag)+exta
;stretch=(mag+0.6)/0.6
DeltaT=DeltaT/stretch
;print, peakmag

While count GE 1. DO BEGIN

      templatet = 60-count
      i = 0.
  mag1=99.99
  mag2=99.99

    While i LT 48. DO BEGIN
        IF (((templatet) GT (data[0,i])) AND ((templatet) LE (data[0,i
+1]))) THEN BEGIN
    ;print, data[0,i]
             a = (data[4,i+1]-data[4,i])/(data[0,i+1]-data[0,i])
             b = data[4,i+1]-a*data[0,i+1]
             mag1 = a*(templatet)+peakmag+b
        END
        i = i+1
    END

  finalt = templatet+DeltaT
  i = 0
</pre>

66

```
      While i LT 48. DO BEGIN
           IF (((finalt) GT (data[0,i])) AND ((finalt) LE (data[0,i+1])))
THEN BEGIN
       ;print, data[0,i]
           a = (data[4,i+1]-data[4,i])/(data[0,i+1]-data[0,i])
               b = data[4,i+1]-a*data[0,i+1]
               mag2 = a*(finalt)+peakmag+b
       END
       i = i+1
    END

    zmag = 0.


    Ft = 10.^(-2./5.*(mag1-zmag))
    Fs = 10.^(-2./5.*(mag2-zmag))
    Rd = zmag-2.5*alog10(abs(Fs-Ft))

    ; IF (Fs GT Ft) THEN BEGIN
   IF (quality EQ 1) THEN BEGIN
     T=0.949
     S=0.579
     Rc=20.718
   endif ELSE IF(quality EQ 2) THEN BEGIN
     T=0.801
     S=0.450
     Rc=20.316
   endif else begin
     T = 0.801
         S = 0.450
         Rc = 20.316
   endelse

         e = T/(1+exp((Rd-Rc)/S))

;    endif ELSE BEGIN
  ;e=0
   ; ENDELSE

   ;print, count, e, Rd, mag1, mag2
   count = count-1

   tc = tc+e
END

return, tc

END
```

Figure A.5: The controltime.pro algorithm. This program is responsible for calculating the Δm_{15} stretch values assuming a typical SNe light curve. It uses light curve data from SN 1994D read from a file.

```
                              dcontroltime.pro

Function dcontroltime, z

filename='/Volumes/iDisk/Public/SGCODE_B/extinction.txt'
read_data_two, data, filename

i= 0
value=0

WHILE i LT 39 DO BEGIN

  IF ((Z GE data[0,i]) AND (Z LT data[0,i+1])) THEN BEGIN
    m = (data[1,i+1]-data[1,i])/(data[0,i+1]-data[0,i])
    b = data[1,i+1] - m*(data[0,i+1])
    value = m*(Z)+b
  END

  i = i+1

END
  return, value
END
```

Figure A.6: The dcontroltime.pro algorithm. This program interpolates the apparent magnitude as a function of redshift. It uses a table obtained via the subroutine read_data_two.pro.

```
                        read_data_two.pro

PRO read_data_two, data, filename

OPENR, 1, filename
data = dblarr(2,40)
readf, 1, data
close, 1
END
```

Figure A.7: The read_data_two.pro algorithm. This program reads in information about the apparent magnitude for a Type Ia SNe at a given redshift.

```
                          extinction.pro

Function extinction, ar

C=5.68087
A=0.0
S=0.2355

prob=exp(-((ar-A)^2)/SQRT(2*S^2))
;prob=C*exp((-(ar-A)/S))

return, prob

END
```

Figure A.8: The extinction.pro algorithm. This program is responsible for defining and integrating over the extinction distribution assumed for galaxies in the local universe.

```
                    probability.pro

Function probability, peakmag


C=0.712397
x=-19.5
o=.56


if peakmag LE -22.0 THEN BEGIN
  prob=0
endif else begin
  prob=C*exp((-(peakmag-x)^2.)/(2.*o^2.))
endelse

return, prob

END
```

Figure A.9: The probability.pro algorithm. This program is responsible for calculating the probability that a SNe will be detected at a given peak magnitude.

```
                          ldensity.pro

Function ldensity, a, z

integral = qsimp('luminosity',a,z)

return, integral

END
```

Figure A.10: The ldensity.pro algorithm. This program is responsible for integrating the luminosity function for galaxies in the local universe over the redshift range provided by the NGSS survey.

```
                        luminosity.pro

Function luminosity, x

h = 0.7    ;constant
Ho = 0.7*100. ;Hubble Constant (km/s/Mpc)
S = 1.     ;Solar Luminosity
O = .000277 ;Degrees surveyed (steradians)
ls = 1.9   ;slope of luminosity density function
c = 3.00*10.^5. ;speed of light (km/s)

result = (2.0*(1.+x)^ls*(10.^8.)*h*S*O*((c/Ho))^3.*x^2.)

return, result

end
```

Figure A.11: The luminosity.pro algorithm. This program defines the luminosity density function.

```
                          read_data.pro

PRO read_data, data, filename

OPENR, 1, filename
data = dblarr(6,49)
readf, 1, data
close, 1
END
```

Figure A.12: The read_data.pro algorithm. This program is designed to read in data from a file that gives baselines for given redshifts.

Bibliography

Blondin, S., et al. 2008, ApJ, 682, 724

Brandt, T. D., Tojeiro, R., Aubourg, É., Heavens, A., Jimenez, R., & Strauss, M. A. 2010, AJ, 140, 804

Cappellaro, E., Evans, R., & Turatto, M. 1999, A&A, 351, 459

Cappellaro, E., Turatto, M., Tsvetkov, D. Y., Bartunov, O. S., Pollas, C., Evans, R., & Hamuy, M. 1997, A&A, 322, 431

Dahlen, T., Mobasher, B., Somerville, R. S., Moustakas, L. A., Dickinson, M., Ferguson, H. C., & Giavalisco, M. 2005, ApJ, 631, 126

Ellis, R. S. 2008, Saas-Fee Advanced Course 36: Cold Aqueous Planetary Geochemistry with FREZCHEM, 259

Ellis, R. 2008, HST Proposal, 11721

Filippenko, A. V. 1997, ARA&A, 35, 309

Gallagher et al. 2008, ApJ, 685, 752

Graves & Schiavon 2008, astro-ph/0803.1483

Hamuy et al. 2000, AJ, 120, 1479

Hicken, M., et al. 2009, ApJ, 700, 331

Howell, D. A., et al. 2009, arXiv:0903.1086

Howell et al. 2009, ApJ, 691, 661

Jha, S., et al. 1999, ApJS, 125, 73

Koleva et al. 2008, MNRAS, 385, 1998

Kennicut 1992, ApJ, 388, 310

Kobayashi et al. 1998, ApJ, 503, L155

Lilly, S. J., Tresse, L., Hammer, F., Crampton, D., & Le Fevre, O. 1995, ApJ, 455, 108

Matheson, T., Kirshner, R. P., Challis, P., Jha, S., Garnavich, P. M., Berlind, P., & Calkins, M. L. 2005, Bulletin of the American Astronomical Society, 37, #171.09

Mannucci et al. 2005, A&A, 433, 807

Matheson, T., et al. 2008, AJ, 135, 1598

Maoz et al. 2010, arXiv:1002.3056

Moaz et al. 2010, arXiv:1006.3576

Maoz, D., Sharon, K., & Gal-Yam, A. 2010, ApJ, 722, 1879

Neff, S. G., Ulvestad, J. S., & Teng, S. H. 2004, ApJ, 611, 186

Pagel et al. 1979, MNRAS, 189, 95

Phillips, M. M. 1993, ApJ, 413, L105

Riess, A. G., et al. 1998, AJ, 116, 1009

Riess et al. 2007, ApJ, 659, 98

Schmidt, B. P., et al. 1998, ApJ, 507, 46

Strolger, L.-G., et al. 2002, AJ, 124, 2905

Strolger, L., Rhoads, J. E., Fruchter, A., Burud, I., Levan, A. J., & Kavelaars, J. J. 2002, GRB Coordinates Network, 1696, 1

Strolger 2003, PhD Thesis, University of Michigan

Strolger et al. 2010, ApJ, 713, 32

Sullivan, M., Ellis, R., Nugent, P., Howell, D. A., Gal-Yam, A., & SNLS Collaboration 2007, Bulletin of the American Astronomical Society, 38, #105.09

Sullivan et al. 2010, MNRAS, 406, 782

Timmes, F. X., Brown, E. F., & Truran, J. W. 2003, ApJ, 590, L83

Tremonti et al. 2004, ApJ, 613, 898

van den Bergh, S., & Tammann, G. A. 1991, ARA&A, 29, 363

Vazdekis et al. 2010 MNRAS, 404, 1639

Vergely, J.-L., Lançon, A., & Mouhcine 2002, A&A, 394, 807

Zwicky, F. 1938, ApJ, 88, 529